

**SYNTHESIS AND CHARACTERIZATION OF  
METHYLAMMONIUM LEAD IODIDE BROMIDE  
PEROVSKITES**



**A Thesis Submitted in Partial Fulfillment of the Requirements for the  
Degree of Master of Science in Physics  
Suranaree University of Technology  
Academic Year 2017**

การสังเคราะห์และการหาลักษณะเฉพาะของเมทิลแอมโมเนียม  
เลดไอโอดด์โบรไมด์เพอร์รอฟสไกต์

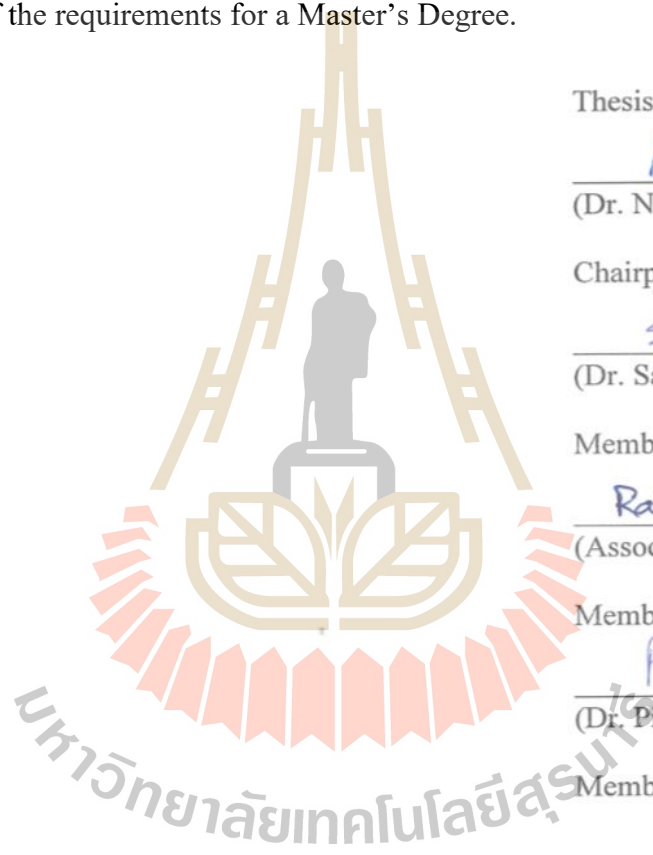


นางสาววิภากร อุตชิสุทธิ

วิทยานิพนธ์นี้เป็นส่วนหนึ่งของการศึกษาตามหลักสูตรปริญญาวิทยาศาสตรมหาบัณฑิต  
สาขาวิชาฟิสิกส์  
มหาวิทยาลัยเทคโนโลยีสุรนารี  
ปีการศึกษา 2560

**SYNTHESIS AND CHARACTERIZATION OF  
METHYLAMMONIUM LEAD IODIDE BROMIDE  
PEROVSKITES**

Suranaree University of Technology has approved this thesis submitted in partial fulfillment of the requirements for a Master's Degree.



Thesis Examining Committee

N. Sanguansak  
(Dr. Nuanwan Sanguansak)

Chairperson

Sroj Rujirawat  
(Dr. Sroj Rujirawat)

Member (Thesis Advisor)

Rattikorn Yimnirun  
(Assoc. Prof. Dr. Rattikorn Yimnirun)

Member

Pinit Kidkhuntod  
(Dr. Pinit Kidkhuntod)

Member

Santi Maensiri

(Prof. Dr. Santi Maensiri)

Vice Rector for Academic Affairs  
and Internationalization

Worawat Meevasana

(Ass. Prof. Dr. Worawat Meevasana)

Dean of Institute of Science

วิทยากร ฤทธิสุทธิ : การสังเคราะห์และการหาลักษณะเฉพาะของเมทิลแอมโมเนียม  
เลดไอโอไดด์โบรไมด์เพอโรฟสไกด์ (SYNTHESIS AND CHARACTERIZATION OF  
METHYLAMMONIUM LEAD IODIDE BROMIDE PEROVSKITES).

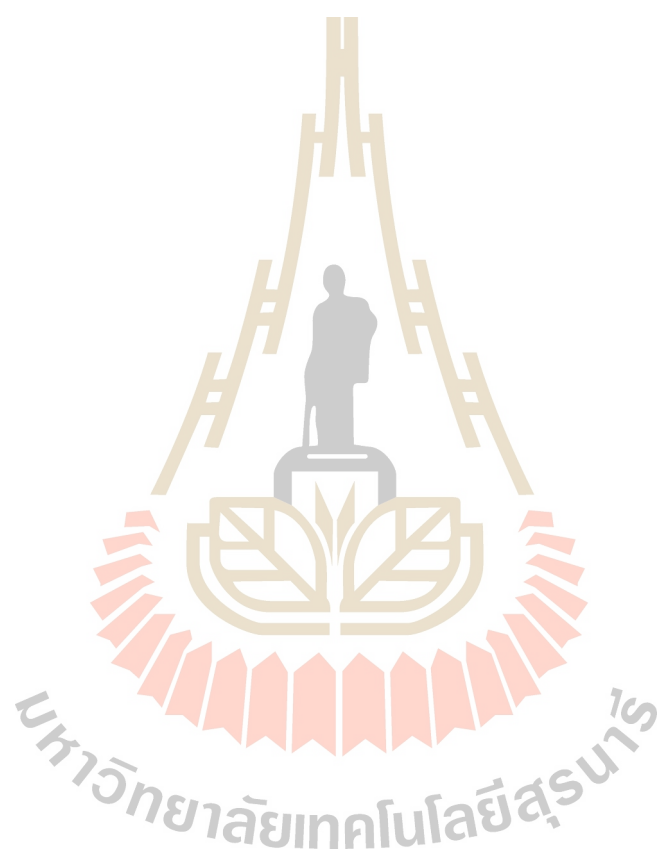
อาจารย์ที่ปรึกษา : อาจารย์ ดร.สาโรช ฐจิรวรรณ, 73 หน้า.

งานวิจัยนี้สนใจศึกษาสมบัติของสารประกอบเพอโรฟสไกด์  $ABX_3$  ซึ่งทำการศึกษา  
ความสัมพันธ์ระหว่างเงื่อนไขที่ใช้ในกระบวนการเตรียม ลักษณะเฉพาะทางโครงสร้าง และสมบัติ  
การดูดกลืนแสง โดยแบ่งเป็นสองส่วนหลัก ๆ ในการอธิบาย

ในส่วนแรกเป็นการศึกษาการเตรียมสารประกอบเพอโรฟสไกด์ของเลดแฮไลด์ในระบบ  
 $ABX_3$  นี้โดยที่ A คือสารอินทรีย์นั่นก็คือ เมทิลแอมโมเนียม B คือสารอนินทรีย์ หรือตะกั่ว และ X  
คือไอออนของธาตุหมู่ 7 (ไอโอไดด์ และโบรไมด์) จะแบ่งการเตรียมออกเป็น 2 ขั้นตอนซึ่งใน  
ขั้นตอนแรกจะเป็นการเตรียมเมทิลแอมโมเนียมไอโอไดด์ด้วยกระบวนการผลิตโดยวิธีโซลเจล เมื่อ  
ได้เกลือ เมทิลแอมโมเนียมไอโอไดด์ ( $CH_3NH_3I$ ) ออกมาจะนำไปสู่ขั้นตอนต่อไปคือการนำตะกั่ว  
โบรไมด์และ เมทิลแอมโมเนียมไอโอไดด์มาเข้าสู่กระบวนการเตรียมผงผลึกด้วยวิธีโซลิดสเตทใน  
อัตราส่วน 1 ต่อ 1 โมล จะได้สารประกอบเพอโรฟสไกด์ ( $CH_3NH_3PbIBr_2$ )

ส่วนที่สองเป็นการศึกษาผลของอุณหภูมิในการอบที่มีผลต่อโครงสร้างและ สมบัติการ  
ดูดกลืนแสงของวัสดุภายใต้เงื่อนไขต่าง ๆ โดยอาศัยผลของ STA เพื่อหาช่วงอุณหภูมิที่เกิดการการ  
เปลี่ยนเฟส พบว่าเสถียรภาพทางอุณหภูมิของสารประกอบเพอโรฟสไกด์อยู่ในช่วงอุณหภูมิ 150 -  
250 องศาเซลเซียส ถ้ามากกว่า 250 องศาเซลเซียส เกลือเมทิลจะสลายตัวทางความร้อน ดังนั้นการ  
เลือกช่วงอุณหภูมิที่ใช้ในการทดลองมีความสำคัญต่อการสังเกตความเปลี่ยนแปลงโครงสร้าง เมื่อ  
ทำการตรวจสอบรูปแบบการเลี้ยวเบนของรังสีเอกซ์ด้วยเทคนิค XRD และดูการเปลี่ยนแปลง  
โครงสร้างจุลภาคจะศึกษาด้วยกล้องจุลทรรศน์อิเล็กตรอนแบบส่องกราด อีกทั้งยังใช้เทคนิคการ  
กระเจิงของรังสีเอกซ์ WAXS ร่วมกับเทคนิคเอกซเรย์โฟโตอิเล็กตรอนสเปกโทรสโกปี XPS มาใช้  
ยืนยันการเปลี่ยนแปลงเฟสที่ได้จากผลการวิเคราะห์ XRD จะพบว่าที่มุมเดียวกันจะให้ข้อมูลของ  
เฟส  $CH_3NH_3I$  ที่ชัดเจนกว่า และ เฟสของ  $PbBr_2$  ที่ยังคงปรากฏอยู่เนื่องจากรังสีเอกซ์ที่ได้แสงจาก  
แสงซินโครตรอนเป็นแสงที่มีความเข้มสูงทำให้ใช้ระยะเวลาในการวัดที่น้อย ส่งผลให้ไม่เกิดความ  
ร้อนสะสมจากการวิเคราะห์ และยังใช้ XRF เพื่อหาอัตราส่วนของ  $Pb:I:Br$  ในตัวอย่างที่เตรียม  
สุดท้ายทำการตรวจสอบสมบัติการดูดกลืนแสงและของสารประกอบ ซึ่งจะทำการศึกษาโดยใช้  
เทคนิคการยูวี-วิสิเบิลสเปกโทรสโกปี Uv-vis พบว่าสารประกอบที่เตรียมได้มีค่าช่องว่าง  
แถบพลังงาน ( $E_g$ ) อยู่ในช่วง 1.79 – 1.89 อิเล็กตรอนโวลต์ ซึ่งทั้งหมดนี้ก็เป็นการศึกษาผลของ

อนุภูมิที่มีต่อโครงสร้างของสารประกอบเพอร์รอฟสไกต์เพื่อนำไปประยุกต์ใช้ในการทำเซลล์  
แสงอาทิตย์ต่อไป



สาขาวิชาฟิสิกส์  
ปีการศึกษา 2560

ลายมือชื่อนักศึกษา จิรัช  
ลายมือชื่ออาจารย์ที่ปรึกษา ศาสตราจารย์ ดร. ชัยวัฒน์  
ลายมือชื่ออาจารย์ที่ปรึกษาร่วม ดร. ชัยวัฒน์

WIPAKORN RITTISUT : SYNTHESIS AND CHARACTERIZATION OF  
METHYLAMMONIUM LEAD IODIDE BROMIDE PEROVSKITES.  
THESIS ADVISOR : SAROJ RUJIRAWAT, Ph.D. 73 PP.

ORGANIC-INORGANIC HALIDE/ X-RAY PHOTOELECTRON  
SPECTROSCOPY

In this thesis work, we are interested in studying the properties of  $ABX_3$  in the perovskites system have been carried out to investigate the relationships existing among conditions of fabricating, structural characteristics and the optical properties. This research have mainly two sections.

The first aim of this work, we will focus on the synthesis of the metal halide perovskites family. All the composition used in this study were prepared based on the perovskite system  $ABX_3$  where A is an organic cation: methylammonium iodide, B is a smaller metal cation: lead (Pb) and X is an anion from the mixed halide between iodide and bromide. However, the preparation of this class of materials is usually divided into two parts: the first step is the preparation of the methylammonium iodide using by sol-gel method and the second step, after the synthesis the dry ammonium salts, we introduce route to prepare the mixing halide compound ( $CH_3NH_3PbI_xBr_{3-x}$ ) was synthesized by solid state reaction method, mixing 1:1 molar ratio of  $CH_3NH_3I$  to  $PbBr_2$ .

Secondly, we report on the effect of annealing temperature on the optical properties of the perovskite compounds. The experimental procedures employed for preparation and characterization of the mixed halide perovskites ( $CH_3NH_3PbI_xBr_{3-x}$ )

compound under the annealing temperature condition was investigated. The thermal stability measurement based on the simultaneous thermal analyzer (STA) indicated that the  $\text{CH}_3\text{NH}_3\text{PbIBr}_2$  compound is stable below  $250^\circ\text{C}$ . This was especially important in select an annealing temperature range in the most suitable condition. The structure and morphology of the products was examined by x-ray diffraction (XRD), analysis of all prepared compounds showed multiple perovskite phase with cubic structure. SEM micrographs showed that as increasing annealed of temperature, the grain size increased. This is also used the wide angle x-ray scattering (WAXS) technique was necessary to confirm the usual low angle structural parameters for our samples. Moreover, we should be checked to the variation of optical properties in compound. Measurement of the amount of absorption can be used to examine the direct bandgap and survival of organic group have been determined using ultraviolet/visible absorption spectroscopy (Uv-vis) and x-ray photoelectron spectroscopy (XPS) respectively. It is concluded that the annealing affects phase formation and thermal stability of  $\text{CH}_3\text{NH}_3\text{PbIBr}_2$ . A small powder amount of lead bromide ( $\text{PbBr}_2$ ), a product of the degradation, was observed with increasing annealing temperature. Accordingly, appropriate annealing temperature should be chosen to produce a high efficiency photovoltaic.

School of Physics

Academic Year 2017

Student's Signature wipakorn

Advisor's Signature Sang Rajirawat

Co-advisor's Signature Redha Yinnich

## ACKNOWLEDGEMENTS

My thesis could not be accomplished without help and support from many people. Especially, I would like to thank my advisors Prof. Dr.Rattikorn Yimnirun and Dr.Saroj Rujirawat for giving me a chance to know materials science and a great privilege to be his student. He is very nice advisor, kind, dedicated. He gave chances to me for joined conference in Japan (IFAAP Hiroshima2018 conference) that gave very valuable experience to me. I would like to my deepest appreciation and thanks to him for his guidance, teaching, encouragement, support, patience and valuable advice. The invaluable lessons that I learned from him are not only in the academics but also in a real life.

I would like to acknowledge Dr. Nuanwan Sanguansak and Dr. Pinit Kidkhunthod, thesis defense committee, for giving their valuable time and guiding good research aspects for my thesis defense and also give me many advices to make me better.

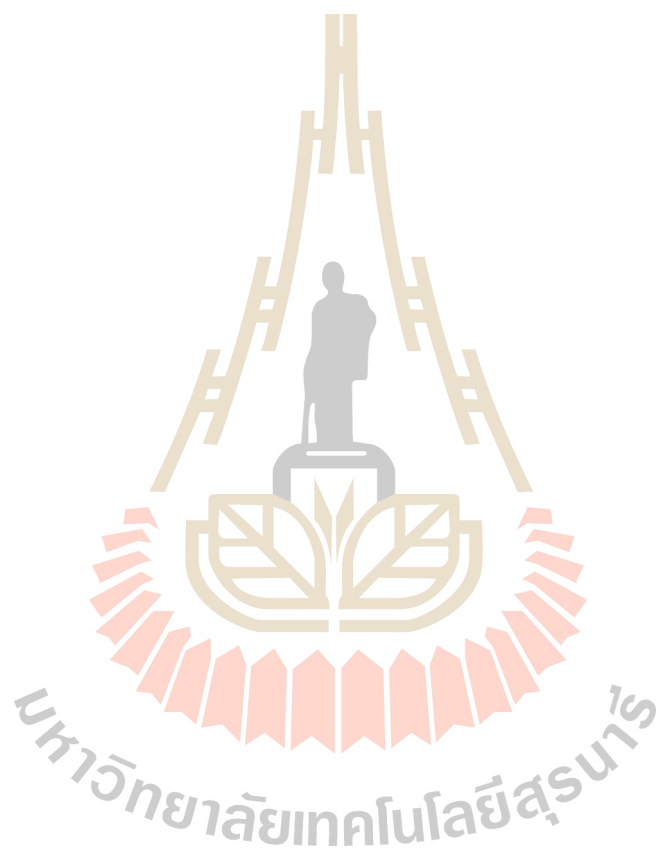
I am thankful to every persons at beamline 5.3 & 1.3 at Synchrotron Light Research Institute (SLRI), Dr. Narong Chenlek, Dr. Siriwat Soontaranon for help in XPS & WAXS measurements.

I would like to big thank Miss Jintrara Patchasi has helped me in completing this thesis from providing technical helps to valuable encouragements.

I would like to acknowledge my scholarship which is the Science Achievement Scholarship of Thailand (SAST) for financial support since bachelor's degree.

And finally, I want to give big thank to every people in Yimnirun group, my family, all teachers and my boyfriend for supporting me to everything which I needed and every time when I have some problems.

Wipakorn Rittisut



# CONTENTS

|  | <b>Page</b> |
|--|-------------|
| ABSTRACT IN THAI .....   | I           |
| ABSTRACT IN ENGLISH .....                                      | III         |
| ACKNOWLEDGEMENTS .....   | V           |
| CONTENTS .....   | VII         |
| LIST OF TABLES .....   | X           |
| LIST OF FIGURES .....  | XI          |
| <b>CHAPTER</b>   |             |
| <b>I INTRODUCTION</b> .....                                    | <b>1</b>    |
| 1.1 Motivation.....  | 1           |
| 1.2 Research objectives.....                                   | 4           |
| 1.3 Scope and limitations.....                                 | 4           |
| <b>II REVIEW OF THE LITERATURE</b> .....                       | <b>6</b>    |
| 2.1 Photovoltaics solar energy .....                           | 6           |
| 2.2 Historical background of solar cell .....                  | 6           |
| 2.2.1 From solid state DSSC to hybrid material solar cell..... | 9           |
| 2.3 The Perovskites.....                                       | 12          |
| 2.3.1 Perovskite structure.....                                | 13          |
| 2.3.2 Recent developments of perovskite applications.....      | 14          |

## CONTENT (Continued)

|   | <b>Page</b> |
|---|-------------|
| <b>III RESEARCH METHODOLOGY</b> .....                           | 25          |
| 3.1 Samples preparation.....                                    | 25          |
| 3.1.1 Powder preparation .....                                  | 25          |
| 3.1.2 Research procedure .....                                  | 29          |
| 3.2 Sample characterizations .....                              | 30          |
| 3.2.1 Simultaneous thermal analysis (STA) .....                 | 30          |
| 3.2.1.1 Thermogravimetric analysis (TGA).....                   | 30          |
| 3.2.1.2 Differential scanning calorimetry (DSC) technique ..... | 31          |
| 3.2.2 X-ray diffraction (XRD) technique.....                    | 32          |
| 3.2.3 Wide-angle x-ray scattering (WAXS) technique .....        | 34          |
| 3.2.4 Scanning electron microscopy (SEM) technique.....         | 35          |
| 3.2.5 X-ray fluorescence (XRF) technique.....                   | 35          |
| 3.2.6 Uv-vis spectrophotometer technique .....                  | 36          |
| 3.2.7 X-ray photoelectron spectroscopy (XPS) technique.....     | 38          |
| <b>IV RESULTS AND DISSCUSSION</b> .....                         | 40          |
| 4.1 Simultaneous thermal analysis (STA) .....                   | 40          |
| 4.1.1 Goldschmidt's tolerance factor .....                      | 43          |
| 4.2 Phase formation by x-ray diffraction (XRD).....             | 45          |
| 4.3 Scanning electron microscopy (SEM) .....                    | 50          |

**CONTENT (Continued)**

|  | <b>Page</b> |
|--|-------------|
| 4.4 Wide angle x-ray scattering (WAXS).....      | 51          |
| 4.5 X-ray fluorescence (XRF).....                | 53          |
| 4.6 Uv-vis spectrophotometer.....                | 54          |
| 4.7 X-ray photoelectron spectroscopy (XPS) ..... | 57          |
| <b>V CONCLUSIONS AND FUTURE RESEARCH.....</b>    | <b>61</b>   |
| 5.1 Conclusions.....                             | 61          |
| 5.2 Suggestions for future works.....            | 62          |
| REFERENCES.....                                  | 63          |
| CURRICULUM VITAE.....                            | 73          |

## LIST OF TABLES

| Table   | Page |
|---|------|
| 2.1 Crystal systems and transition temperatures of $\text{CH}_3\text{NH}_3\text{PbX}_3$ (X=Cl, Br, I).....  | 17   |
| 4.1 Ionic radii used to calculate tolerance factor of hybrid perovskite.....  | 44   |
| 4.2 The crystallographic structural data of $\text{CH}_3\text{NH}_3\text{PbIBr}_2$ diffraction peak of full width at half-maximum and crystallite size of the XRD pattern. .... | 48   |
| 4.3 The particle size of $\text{CH}_3\text{NH}_3\text{PbIBr}_2$ .....   | 51   |
| 4.4 Weight percentage values for the elements in the samples prepared, obtained by means of XRF technique. ....   | 53   |
| 4.5 The data band gap of samples.....   | 55   |

## LIST OF FIGURES

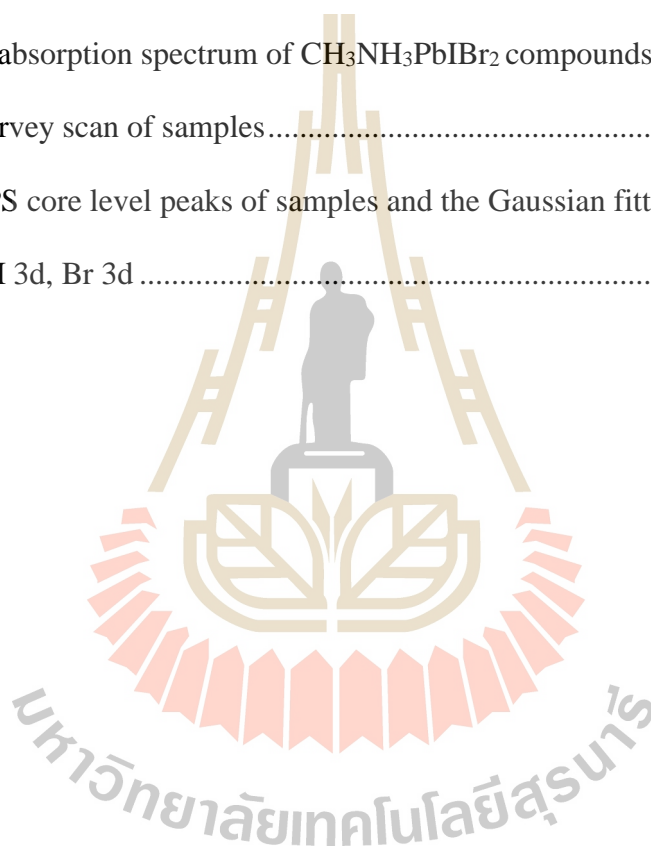
| Figure   | Page |
|--|------|
| 1.1 World energy usage in 2016 (mathematic data is from: key world energy statistics 2016, International energy agency).....   | 1    |
| 2.1 This diagram shows the wavelength and frequency ranges of electromagnetic radiation .....  | 7    |
| 2.2 Schematic showing the relationship between cell efficiency and cost for the three generations of solar cells, with the dotted lines showing the trajectories for different cost per watt. .... | 9    |
| 2.3 Schematic diagram representing components and working mechanism of the DSSC .....  | 10   |
| 2.4 Configuration of various types of perovskite solar cells .....   | 11   |
| 2.5 Timeline of research solar cell efficiency .....   | 12   |
| 2.6 Perovskite aristotype structure.....   | 14   |
| 2.7 Overview of the application procedure and the ions calculated.....   | 23   |
| 3.1 The schematic diagram of the substrate $\text{CH}_3\text{NH}_3\text{I}$ compound .....   | 26   |
| 3.2 The sample powder of $\text{CH}_3\text{NH}_3\text{PbI}_2$ perovskites .....  | 27   |
| 3.3 The schematic diagrams for research procedure .....  | 29   |
| 3.4 Thermogravimetric analyzer.....  | 31   |
| 3.5 Differential scanning calorimetry .....  | 31   |
| 3.6 X-ray diffraction (XRD) .....  | 32   |

## LIST OF FIGURES (Continued)

| <b>Figure</b>   | <b>Page</b> |
|---|-------------|
| 3.7 The schematic representation of XRD characterization principle.....   | 33          |
| 3.8 WAXS experimental which BL1.3 set up at the siam photon laboratory,<br>synchrotron light research institute .....   | 34          |
| 3.9 Scanning electron microscopy (SEM) used in this study.....  | 35          |
| 3.10 X-ray fluorescence spectroscopy at synchrotron light research institute .....  | 36          |
| 3.11 Uv-vis spectrophotometer at synchrotron light research institute .....   | 37          |
| 3.12 XPS experimental which BL5.3 at synchrotron light research institute .....   | 38          |
| 4.1 Thermogravimetric analyses of methyl ammonium iodide ( $\text{CH}_3\text{NH}_3\text{I}$ ),<br>methylammonium lead iodide-bromide ( $\text{CH}_3\text{NH}_3\text{PbIBr}_2$ ) and lead bromide<br>( $\text{PbBr}_2$ ), showing the higher thermal stability of the inorganic perovskite<br>compared to the hybrid organic-inorganic perovskite..... | 41          |
| 4.2 TGA heating curves of individual precursor powders expressed as weight %<br>as a function of applied temperature and the corresponding first derivatives ...  | 43          |
| 4.3 The XRD patterns of the samples powder following annealing at various<br>temperatures .....   | 46          |
| 4.4 The XRD patterns present the diffraction peak of full width at half-maximum<br>(FWHM). .....  | 49          |
| 4.5 SEM images of $\text{CH}_3\text{NH}_3\text{PbIBr}_2$ compounds that have been thermally annealed<br>at various temperatures at (A) $150^\circ\text{C}$ , (B) $200^\circ\text{C}$ , (C) $225^\circ\text{C}$ , (D) $250^\circ\text{C}$ .....  | 50          |

**LIST OF FIGURES (Continued)**

| <b>Figure</b>  | <b>Page</b> |
|--|-------------|
| 4.6 WAXS images of $\text{CH}_3\text{NH}_3\text{PbIBr}_2$ compounds.....                                     | 52          |
| 4.7 Uv-vis absorption spectrum of $\text{CH}_3\text{NH}_3\text{PbIBr}_2$ compounds .....                     | 56          |
| 4.8 XPS survey scan of samples.....  | 57          |
| 4.9 The XPS core level peaks of samples and the Gaussian fitting for C 1s, N 1s,<br>Pb 4f, I 3d, Br 3d ..... | 58          |



# CHAPTER I

## INTRODUCTION

### 1.1 Motivation

Today, the demand for clean and renewable energy has grown steadily over time. Which the main source of energy comes from fossil fuels and the dominant fossil fuels currently used by most industrialized and developing countries are oil, coal, and natural gas. Among these fossil fuels, oil is most commonly used for energy conversion, followed by coal for natural gas.

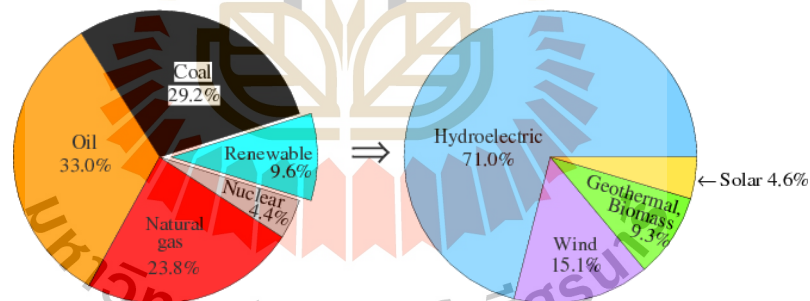


**Figure 1.1** World energy usage in 2016 (mathematic data is from: key world energy statistics 2016, international energy agency).

Fossil fuels have advantages such as high combustion and high efficiency, but also a serious environmental problem. The emitting gas includes CO<sub>2</sub>, NO, SO<sub>2</sub>, poly aromatic, etc. According data analysis of IEA, fossil fuel contributes to 99.5% of total

amount of CO<sub>2</sub> is believed to be responsible for global warming. Which as fossils continued to be depleted, establishing the alternative forms of energy has become paramount to compensate the effects climate change and reduce of dependence on carbon dioxide emitting fuels. Harvesting solar energy has been identified as a key to solving this problem. Photovoltaic power has been a lot of attention due to alternatives energy deployment targets and CO<sub>2</sub> emission control. The development of the new technologies and materials could lead to the reduction of photovoltaic electricity generation cost. If photovoltaic power is to be the main source of energy, it must be collected and converted into a simple and largely used energy forms to meet the needs of daily life. Organic- inorganic hybrid perovskite materials present promising way for the development of low-cost solar cell able to global energy. The perovskites solar cells are a variation on dye sensitized solar cell, which a solid metal halide dye is used as good light absorber and capable of generating a high photocurrent.

Organic–inorganic hybrid perovskite materials are interesting semiconductors for photovoltaics because their very simple process, low-cost, low-temperature processing for production and high power conversion efficiencies. The name of perovskite material has general chemical formula ABX<sub>3</sub> structure, where A is an organic cation, B is a smaller metal cation and X is an anion from the halide (such as iodine, bromine or chlorine) or co-existence of several halogens. Which the high efficiencies have mostly been achieved using methylammonium lead halide based perovskites by the halide is an iodide. The most widely studied CH<sub>3</sub>NH<sub>3</sub>PbI<sub>3</sub> is very well known material which has the properties for solar cell applications, good absorber material, which determines its absorption offset up to 800 nm, exciton binding energy of merely 0.03 eV and high efficiency reaching up to 20.1%. But, the unstable nature in these materials remains a

major challenge path to development of commercially practicable perovskite base solar cell. Mixing halides is anticipated to resolve this problem. The most favorable try to improve the material instability of  $\text{MAPbI}_3$  is to replace I ions (a direct bandgap of 1.55 eV) with Br ions (direct bandgap of 2.2 eV). Noh and co-workers (Noh et al., 2013) were demonstrate the bandgap of these materials can be tuned due to mixing iodide and bromide. Interestingly, bromide-containing perovskites were found to show better stability under moist air condition. Mixed-halide iodide–bromide perovskites are an important material class that can allow a 1.75 eV (Eperon et al., 2016) bandgap crucial for integration with silicon in tandem cells. Another very important, the annealing can be improve the performance of the solar cell devices. It is found that thermal annealing not only drives the formation of perovskite but also affects the morphology. Thermal annealing is technique to increase the grain size and crystallinity of materials especially thin films because of its simplicity. Annealing at high-temperatures for short times or low-temperature thermal annealing for longer periods has been some reported to decompose the perovskite films and so abate the device efficiency. However, increasing the annealing temperature too high leads to the supplementary formation of lead-halide which, is dangerous to the photovoltaic performance.

Hence, in this work we focus on the synthesis of this particularly promising class of crystalline organic-inorganic mixed-halide perovskite  $\text{CH}_3\text{NH}_3\text{I}$  compound by sol-gel method and preparation of  $\text{CH}_3\text{NH}_3\text{PbIBr}_2$  compound by solid-state reaction method. The effect of the annealing temperature condition was investigated. Then, the compounds were analyzed using various characterization techniques. Considering thermal stability which is also an important property for halide perovskites for the new applications, we carried out thermogravimetric and differential scanning calorimetry

(TGA-DSC) analysis of the as-prepared  $\text{CH}_3\text{NH}_3\text{PbIBr}_2$  powder sample. We can structurally analyze using techniques such as x-ray diffraction (XRD), wide angle x-ray scattering (WAXS) to make it possible to correlate structural features with specific materials properties. Moreover, the x-ray fluorescence (XRF) technique was used in this work to determine the elemental composition of perovskites compound. To check the variation of optical properties in these compound, we measured the uv-visible absorption spectroscopy and x-ray photoelectron spectroscopy (XPS) to examine the direct bandgap and the survival of organic group. Consequently, appropriate annealing temperature should be chosen to produce a high efficiency photovoltaic.

## 1.2 Research objectives

The objectives of this research are as follows:

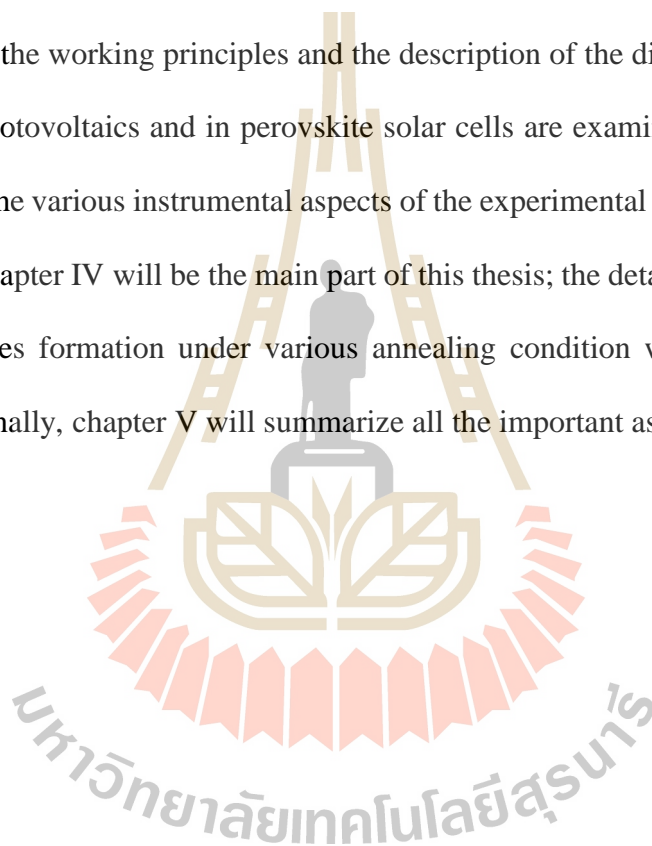
1. To examine the possibility of synthesizing  $\text{CH}_3\text{NH}_3\text{PbIBr}_2$  compound.
2. To synthesize and characterize of  $\text{CH}_3\text{NH}_3\text{PbIBr}_2$  powders in terms of structure using advanced characterization tools.
3. To study the optical properties of the  $\text{CH}_3\text{NH}_3\text{PbIBr}_2$  compound by light absorption technique.
4. To investigate the properties of the synthesized  $\text{CH}_3\text{NH}_3\text{PbIBr}_2$  compound in relation to its application in solar cells.

## 1.3 Scope and limitations

1. This study focuses on the synthesis of  $\text{CH}_3\text{NH}_3\text{I}$  compound by sol-gel method and preparation of  $\text{CH}_3\text{NH}_3\text{PbIBr}_2$  compound by solid-state reaction method.

2. The phase identification, structure characterization and the effect of temperature on the synthesized compound will be investigated using TGA-DSC, XRD, SEM, WAXS, XRF, Uv-vis and XPS techniques.

Based on these objectives, the next chapter will start with the literature review. The chapter II is dedicated to the detailed description of the new generation solar cells. In particular, the working principles and the description of the different materials used in organic photovoltaics and in perovskite solar cells are examined. Then, chapter III will explain the various instrumental aspects of the experimental measurements used in this work. Chapter IV will be the main part of this thesis; the detailed measurements of the perovskites formation under various annealing condition will be explained and discussed. Finally, chapter V will summarize all the important aspects of this work.



## **CHAPTER II**

### **REVIEW OF THE LITERATURE**

This chapter suggests the theory behind perovskite solar cells and basic operation principles of photovoltaics. To understand the origin of their photovoltaics performance and accelerate the search for new materials, it is important to first understand the crystal structures of the methylammonium lead halide perovskites, characterized by structural phase transitions of various defects such as halogen anion or organic cation vacancies. The development of solar cells from the first generation solar cells to perovskite solar cells is then described, together with their operation. Finally, which demonstrate excellent photovoltaic performance in solar cells to improve the device performance and develop new applications.

#### **2.1 Photovoltaics solar energy**

Solar cells is the direct conversion of sunlight directly into electricity by converting photons (light particles) into electrons (negatively charged particles). This is done using a principle known as the photovoltaic effect. Some materials show a property known as the photoelectric effect that causes them to absorb photons of light and release electrons. When these free electrons are captured, an electric current results that can be used as electricity. Photovoltaic cells are made of semiconductors and silicon mixed with other material.

## 2.2 Historical background of Solar cell

The sun is the major source of ultraviolet, visible, and infrared radiation. The word light is used commonly to identify the portion of the electromagnetic radiation spectrum that is visible to the human eye, which the electromagnetic radiation comes from the sun and transmitted in waves or particles at different frequencies and wavelengths. A typical human eye will respond to the wavelength range from 390 to 750 nm, lying between the ultraviolet and infrared wavelengths Figure 2.1.

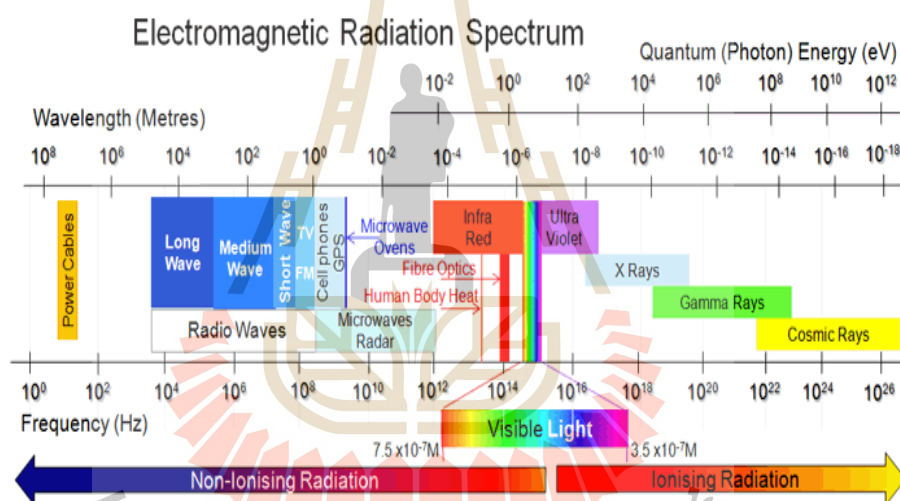


**Figure 2.1** This diagram shows the wavelength and frequency ranges of electromagnetic radiation (Kim et al., 2012).

The sun is considered to produce a constant amount of energy, at the surface of the sun the intensity of the solar radiation is about  $1.7 \times 10^5$  TW. According to an energy information agency estimate, we humans produced and used  $5.67 \times 10^{20}$  joules of energy in 2013, equivalent to about 18.0 terawatts. From 2000–2013 coal was the source of energy with the largest growth. The use of oil and natural gas also had

considerable growth, followed by hydropower and renewable energy. Renewable energy grew at a rate faster than any other time in history during this period. The earthly solar energy is remarkably higher. Beyond, sunlight is without cost, unlimited, readily available, clean, and all over the place. This makes the solar energy one of the most interest technologies to meet the energy needs. Which the history of solar cells can be divided in three parts, according to the evolution of technology. The first generation of solar cell was based on crystalline silicon materials, which relatively high cost but also high efficiency single junction cells, their record efficiency is 25.6%. However, the main problem for this technology was the demand for high volume of starting materials. Next generation of solar cells was developed from the early 1980s, these solar cells used amorphous silicon and alternative inorganic materials including multi-junction thin silicon film, cadmium telluride (CdTe) thin film, copper, indium, gallium, selenide/sulphide (CIGS) and copper, indium, selenide/sulphide (CIS) as photoactive semiconductor, using thin film technology reduces costs by produce per square metre but are also lower efficiency than the crystalline silicon cells. Both first and second generations are single junction cells. Organic photovoltaic (OPV) cells are also sometimes referred to as third generation. The third generation seeks to breach this single junction limit through either multi-junction cells or other devices that can capture the energy from hot electrons. The cost per square metre is similar to the second generation succeed at lower cost per watt through gaining higher efficiency, which included dye sensitized solar cell (DSSC), organic photovoltaic cell (OPV), quantum dot solar cell, and the recently developed perovskite solar cell.

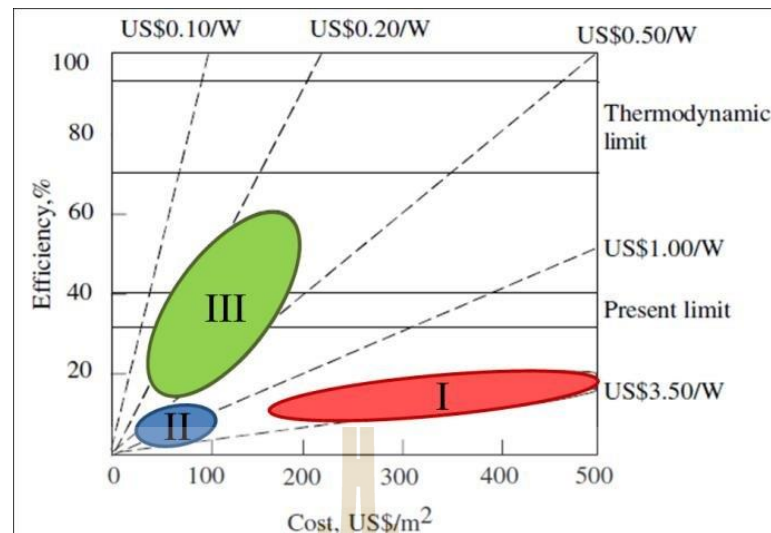


**Figure 2.2** Efficiency-cost trade-off for the three generation of solar cells.

The dye sensitized solar cell and organic photovoltaic cell systems have been continuously developed for more than decade. The most attractive properties of DSSCs are their low-cost and simple manufacturing processes together with their advantageous attributes such as lightweight, low toxic, and good performance in diverse light conditions. The solar cell products can also be flexible, using transparent conductive oxide (TCO) coated plastic substrate. However, the conversion efficiency of these cells will remain low compared to the first and second generation solar cells. In addition, durability, lifetime, stability, and lifetime of these cells have not been improved before the actual application becomes available.

### 2.2.1 From solid state DSSC to hybrid material solar cell

Among the various types of new generation photovoltaic, dye sensitized solar cell is considered interesting, DSSC uses dye as a light absorber. The photo-excited electron from the excited dye was then transported through the  $\text{TiO}_2$  layer toward the electrode, while the excited dye accepted electrons from  $\text{NaI/I}_2$  electrolyte before

returning to ground state (in Figure 2.3). However, stability and lifetime of the DSSC have yet to be further improved. This is attributed to the fact that liquid electrolyte and solvents used in the DSSC are often evaporated and leak out of the cell. Alternatively, a kind of room temperature ionic liquid (RTIL) might be used as a displacement of the liquid electrolyte. However, the leakage issue still exists if an adhesion between a sealing film and glass substrate was strong enough.

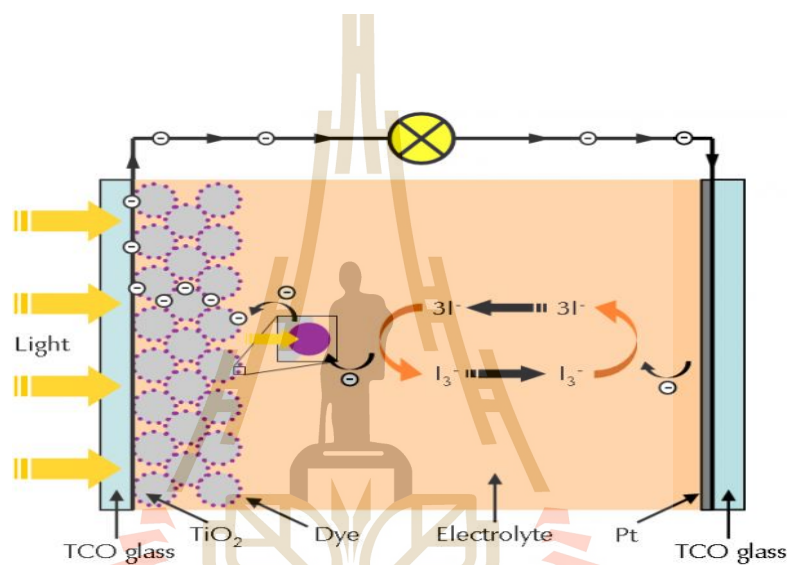


**Figure 2.3** Schematic diagram representing components and working mechanism of the DSSC.

Therefore, the trend of research and development in the next stage is focused on the use of the solid and quasi-solid (gel) electrolytes. This include various types of hole transport materials (HTM) such as Spiro- OMeTAD, CsSnI<sub>3</sub> and P<sub>3</sub>HT. It was also the stability of the DSSC containing solid electrolyte is often improved at the expense of its power conversion efficiency. Because, the use of solid HTM still has some limitations in terms of pore-filling or contact between HTM and the electrode. Consequently, endeavors have been made to use 1D TiO<sub>2</sub> as a replacement of

mesoporous  $\text{TiO}_2$  (Figure 2.4, middle). Interestingly, work by Snaith (Snaith et al., 2013) shown that by using easy configuration of the cell (Figure 2.4, right), power conversion efficiency of the perovskite solar cell as high as 10% can be received, provided that morphology of the active layer must be uniform and dense. Furthermore, Lee (Lee et al., 2015) revealed that apart from functioning as a light absorber then the perovskite can also serve as an electron acceptor. This introduces that the perovskite solar cell can be a kind of mesoporous  $\text{TiO}_2$ -free cell. In this regard, it was possible that the annealing step at high temperature can be remove and so the use of plastic substrate made from PET or poly (ethylene naphthanate) can be more realized.

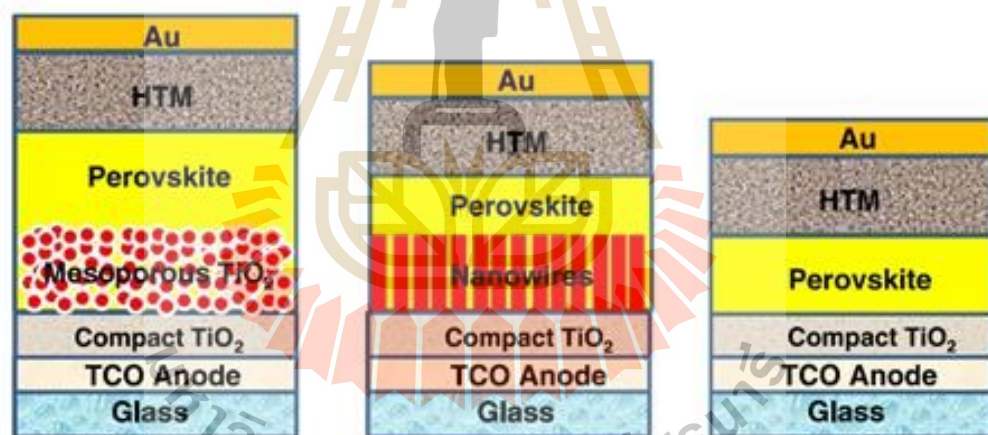


**Figure 2.4** Configuration of various types of perovskite solar cells.

In that case, perovskite layer was deposited on top of the meso-porous  $\text{TiO}_2$  layer and the photoactive material was sandwiched between Au and FTO. Consideration of the literature review in this field during 1990 to 2015 reveals that power conversion efficiency of perovskite solar cells have been improved rapidly as compared to those of other new generation solar cell analogues. Until now, the power conversion efficiency

as high as 21.4% (far exceeding that of DSSC and compare with other thin film technologies such as CdTe and CIGS, as shown in Figure 2.5) was claimed and it seems that the raising trend is ongoing.

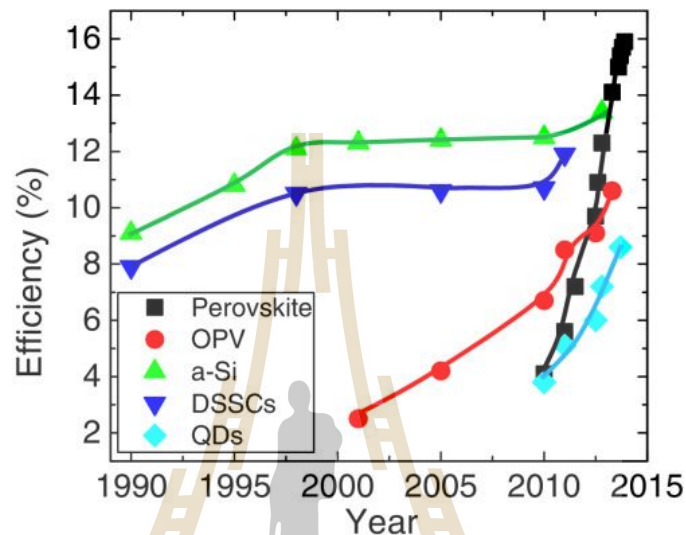


**Figure 2.5** Timeline of research solar cell efficiency.

A new group of materials has emerged as a potential candidate for solar cells production in the last decade. Perovskite is the name of a crystal structure, which the first found in the original mineral structure is calcium, titanium and oxygen in the form  $\text{CaTiO}_3$ . A few review papers have been published on oxide and halide based perovskites with importance on solar cell application.

### 2.3 The Perovskites

The research field of perovskite solar cells has recently been developed as the most promising candidate for the fourth generation high efficiency solar cell technology this is compatible with low-cost, low-temperature processing, long-term stability and

simple structure of solar cells production. The trend of highest efficiency achieved by DSSC comparing with other photovoltaic technologies over time is shown in Figure 2.5. Organo-metal halide perovskite material was first produced in 2009 (Kojima et al., 2009), while the perovskite materials provide useful features of both organic and inorganic materials, such as plastic mechanical properties (organic material) and good electronic mobility (inorganic material). One of the highlighting important properties of the organic–inorganic perovskite for their use in photovoltaics cells is the possibility to tune their optical properties.

### 2.3.1 Perovskite structure

The terms perovskite structure has the generic form  $ABX_3$ , a similar form structure to oxide perovskites such as calcium titanate. The structure shows a huge possibility on element substitutions on A, B and X site. A presents an organic cation, B presents a metal cation and X is a halide anion. Currently, the most of the studied perovskite solar cells are based on methylammonium lead trihalide perovskite. In these systems, A is a small organic dipolar cation such as methylammonium (MA,  $CH_3NH_3^+$ ), formamidinium (FA,  $HC(NH_2)_2^+$ ), B is a divalent metal cations such as  $Pb^{2+}$ ,  $Ba^{2+}$ ,  $Sn^{2+}$  coordinate with 12 and 6 forming cuboctahedral and octahedral geometries respectively (Figure 2.6) and X is an anion from the halide ( $Cl^-$ ,  $Br^-$ ,  $I^-$ ) or co-existence of several halogens. The distortion results in lower-symmetry structures and may also shows rise to many interesting and useful properties such as ferroelectricity, antiferroelectricity, band-gap tune ability, high carrier mobility sunlight, a balanced electron and hole transport, high power conversion efficiencies and large absorption coefficients (Fu et al., 2015; Mitzi et al., 1995). Another very important advantage is that they can be prepared through a variety of different processing technologies such as vacuum,

solution-based techniques and specially, the uncomplicated low-temperature solution process ability makes metal halide perovskite semiconductors that interesting. Based on these assets, metal halide perovskite can already be regarded as a potential low cost alternative for silicon-based solar cell.

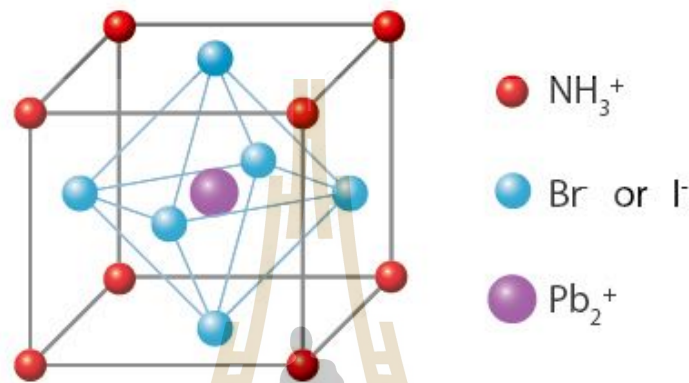


**Figure 2.6** Perovskite aristotype structure: cubic unit cell with A-cation (red),  $\text{BX}_6$ -octahedra (B-cation - purple and X-anion - blue).

Consequently, improving the crystallization and morphology of metal organic perovskites, chemical management of compositional elements has been verified as an effective toward further adjust the properties. An important characteristic of the most commonly used perovskite system, the methylammonium lead halides is a bandgap controllable by the halide content and the mixture of multiple halide elements in organic metal can bring at the perfect perovskite.

### 2.3.2 Recent developments of organolead perovskite-based applications

The mineral perovskite is composed of calcium, titanium and oxygen in the form  $\text{CaTiO}_3$ . Many studies have been published on oxide and halide based perovskites with importance on solar cell application in many fields such as sensors (Atta et al., 2016),

super conductors (Dogan et al., 2015), fuel cell (Boukamp et al., 2003), ferroelectrics and thermoelectric (Atta et al., 2016). The new group of rediscovered members of this family, organo-lead halide perovskites turned out to be trending component of solar cell (Kojima et al., 2009). Consequently, the perovskite solar cells have attracted enormous interest as the most remarkably growing photovoltaic devices. A new record certified non-stabilize power efficiencies has exceeded 22% in 2016 achieved by Seok's group (KRICT/UNIST, South Korea), although the device was not stabilized. Indeed, rapid X= halide group (Yang et al., 2004) exchange has been demonstrated and is now widely used in thin films and nanocrystals with different morphology, such as nanowires (Horváth et al., 2014; Spina et al., 2016), fiber-shaped (Lee et al., 2015), nanoparticles (Schmidt et al., 2014), nanocrystal (Kumar et al., 2016), hydrothermal method (Xia et al., 2015). Then, there are some warning signal associated with the various components of the  $\text{CH}_3\text{NH}_3\text{PbX}_3$  based the perovskites material show unstable properties which affects the chemical instability dramatically restricts the commercial development in the future. So it should be understood the basis for the degradation of PSCs and solve it which some factors have been investigated air (moisture and oxygen) stability, photo stability and thermal stability. All of these factors should be taken into judgment for a high stability PSC (Kim et al., 2012). This wide-ranging improvement in performance is due both to improved synthesis of defect perovskite structure and to the engineering of electron and hole selective contacts that enable efficient charge separation. While a few startup companies seek to commercialize solar cells based on methylammonium lead iodide ( $\text{CH}_3\text{NH}_3\text{PbI}_3$ ) as early as 2017, primary research on perovskites is still succeeding with the goal of explain the mechanisms of absorption and charge transport that provide hybrid perovskites such intriguing potential. To take advantage of the solar

cells more and better, first it is necessary that we have comprehensive information on the microscopic properties of absorbent layer. The results of experimental research show that due to temperature, pressure or external field changes (Brivio et al., 2013; Baikie et al., 2013) and variation of type and size in organic cation (Amat et al., 2013), phase transition (Wang et al., 2013) and consequently the structural properties would change. Which the three main of perovskites compounds  $\text{CH}_3\text{NH}_3\text{PbI}_3$ ,  $\text{CH}_3\text{NH}_3\text{PbBr}_3$ ,  $\text{CH}_3\text{NH}_3\text{PbCl}_3$  should know the basic properties. For example, the direct band gap of semiconductors with a high absorption coefficient among which  $\text{MAPbI}_3$  gives a bandgap 1.55 eV,  $\text{MAPbBr}_3$  2.2 eV, and  $\text{MAPbCl}_3$  3.0 eV (Eperon et al., 2014; Noh et al., 2013; Nguyen et al., 2015). However, structural and electronic differences between the three materials, such as the exact role of I, Br and Cl anions have yet to be undoubtedly determined by the community. The researcher observed that incorporation of I, Br and Cl as a dopant can improve the charge transport within the perovskites layer, improve the stability of the cell in room temperature and increase the performance of the photovoltaic and optical properties. Which found that the perovskite structure have provide structural transition upon heating. The systems and transition temperatures are summarized in Table 2.1, as reported in the previous works (Jung et al., 2015; Knop et al., 1990).  $\text{CH}_3\text{NH}_3\text{PbX}_3$  (X= Cl, Br, I) is the cubic perovskite structure with the unit cell parameters  $a = 5.68$  (X= Cl),  $a = 5.92$  (X= Br) and  $a = 6.27$  (X= I). With exception of  $\text{CH}_3\text{NH}_3\text{PbCl}_3$ , the compounds show intense color, but there is no significant conductivity under normal conditions (Weber et al., 1978). But, my research interests focus on two perovskites compound that methylammonium lead triiodide and methylammonium lead tribromide.

**Table 2.1** Crystal systems and transition temperatures of  $\text{CH}_3\text{NH}_3\text{PbX}_3$  (X=Cl, Br, I).

| Material                   | $\text{CH}_3\text{NH}_3\text{PbCl}_3$ | $\text{CH}_3\text{NH}_3\text{PbBr}_3$ | $\text{CH}_3\text{NH}_3\text{PbI}_3$ |
|----------------------------|---------------------------------------|---------------------------------------|--------------------------------------|
| Crystal system             | Cubic                                 | Cubic                                 | Cubic                                |
| Transition temperature (K) | 177                                   | 236                                   | 330                                  |
| Crystal system             | Tetragonal                            | Tetragonal                            | Tetragonal                           |
| Transition temperature (K) | 172                                   | 149-154                               | 161                                  |
| Band gap (eV)              | 3.0                                   | 2.3                                   | 1.55                                 |

Perovskite materials constitute a very important compound is methylammonium lead triiodide ( $\text{CH}_3\text{NH}_3\text{PbI}_3$ ) showing a multitude of properties including insulating, semiconducting, conducting and superconducting. Among the methylammonium lead iodide ( $\text{MAPbI}_3$ ) were currently the champion materials with ~22% record efficiencies. This material has ideal properties for solar cell applications such as (Snaith et al., 2013; Xing et al., 2013) independently reported the diffusion length measurements performed on hybrid perovskites, which presented that the effective diffusion lengths are indeed relatively large in  $\text{CH}_3\text{NH}_3\text{PbI}_3$  films, long carrier diffusion lengths (100 nm to 1  $\mu\text{m}$ ) for both electrons and holes a high value for a semiconductor formed from solution at low temperature. The highly efficient solar cell should be able to absorb over a wide range of spectra, from visible to near infrared wavelengths (320-1000 nm), converting the incident photon energy effectively into movable charges. Hence, the electronic structure of a solar energy harvester should have a suitable optical band gap, enabling absorption of different photons in the solar spectrum. Moreover, the high mobility of

carriers is important, because it requires that the light-generated electrons and holes can move large enough distances to be extracted as current, instead of losing their energy as heat within the cell and high mobilities for electrons ( $7.5 \text{ cm}^2\text{V}^{-1}\text{s}^{-1}$ ) and holes ( $12.5\text{--}66 \text{ cm}^2\text{V}^{-1}\text{s}^{-1}$ ). The perfect structure of perovskite material allows optimal band gap of 1.5 eV with a very sharp absorption edge, which determines its absorption offset up to 800 nm. But, it also turned out that  $\text{MAPbI}_3$  suffers from the poor material stability, which presents a challenge to development of commercially viable perovskite solar cells. However, we found that the perovskite can be easily decomposed when exposed to humidity, high temperature, and extended period of light exposure. Therefore, hermetically sealed packaging is difficult to survey the humidity-induced degradation, the thermal-induced degradation remains the biggest challenge for the viability of perovskite solar cells, specifically under continued exposure to sunlight. Recent reports show the thermal stability of the  $\text{MAPbI}_3$  is considerably affected by the manufacture routes used to make perovskite solar cell devices.

In this second part, they explore the surface properties of the  $\text{CH}_3\text{NH}_3\text{PbBr}_3$  perovskite photovoltaic material. This compound has a large bandgap of 2.2 eV and is a suitable candidate for the top cells of all perovskite tandem cells because the dominant defects in  $\text{CH}_3\text{NH}_3\text{PbBr}_3$  create only shallow levels. These unusual defect properties are largely due to the strong Pb lone-pair s orbital and Br p orbital anti-bonding coupling and high ionicity ionic of  $\text{CH}_3\text{NH}_3\text{PbBr}_3$  perovskites. Recent reports have shown that  $\text{CH}_3\text{NH}_3\text{PbBr}_3$  exhibits a unipolar self-doping behavior, this is it can be grown with only excellent p-type conductivity under thermal equilibrium growth conditions. However, there is continued need for understanding of these materials for their research, Edri and co-workers reported in spite of the 1.3 V  $V_{\text{OC}}$  (Edri et al.,2013),

mesoscopic alumina MAPbBr<sub>3</sub>/NN'-dialkyl perylenediimide (PDI) solar cells, but the efficiency was below 1%. Subsequently, Qiu 's group have attained 3.04% power conversion efficiency and V<sub>oc</sub> of 1.16 V in mesoscopic TiO<sub>2</sub>. Very recently, Ryu (Ryu et al., 2008) has reported a 6.7% efficiency and V<sub>oc</sub> of 1.4 V in mesoscopic TiO<sub>2</sub>/MAPbBr<sub>3</sub>/poly-indenofluoren-8-triarylamine (PIF8-TAA). Thus, the device efficiencies of MAPbBr<sub>3</sub> perovskite solar cells are not high enough for use in the production of solar fuel or as top cells for tandem devices. Which, it may be assembled by the factor that deposition of dense MAPbBr<sub>3</sub> thin-films was not optimized because the probability of recombination between the electron conductor and hole conductor can be vastly suppressed by a pinhole-free MAPbBr<sub>3</sub> light absorbing interlayer. Our results suggest that CH<sub>3</sub>NH<sub>3</sub>PbBr<sub>3</sub> can be a good absorber for achieving an open circle voltage as 1.5 eV with 10.4% power conversion efficiency for CH<sub>3</sub>NH<sub>3</sub>PbBr<sub>3</sub> based thin-film cells by Ryu (Ryu et al., 2008) as well as a good candidate for low-cost hole-transport material for lead halide perovskite solar cells. Great effort has been attentive to produce large-grained perovskite films, improving their crystalline quality. In single crystal of methyl ammonium lead tribromide (MAPbBr<sub>3</sub>), carrier diffusion lengths over 100 nm and bulk trap state densities of the order of 10<sup>9</sup> to 10<sup>10</sup> per cubic centimeter have been indicated (Green et al., 2014; Heo et al., 2015).

In this rapidly evolving situation, many papers have been focusing on material properties directly related to device performance as determined by the use of different perovskite materials and synthetic procedures, hole transporting materials, photoanodes and solar cell structures as shown in several reviews. The research have found that MAPbI<sub>3</sub> is more sensitive to moisture and humidity than MAPbBr<sub>3</sub> but the absorption of MAPbBr<sub>3</sub> is not comparable to that of MAPbI<sub>3</sub>. Consequently, some researchers

focused on the preparation of mixed halide group in the perovskites  $\text{MAPbI}_{3-x}\text{Br}_x$  and  $\text{MAPbI}_{3-x}\text{Cl}_x$ . In terms of chemical composition in halide group makes the halide perovskites an extremely interesting family of materials. For example, the research made substitution for iodine with chloride or bromide atoms in bulk  $\text{MAPbI}_3$  leads to a significant improvement of perovskite stability. Although, there are many studies on the growth of mixed halide bromine perovskite, their formation process remains poorly investigated. Their properties, such as bandgap, which can be tuned with appropriate composition control, increase the range of applications to beyond conventional photovoltaics such as large bandgap halide perovskites using  $\text{Br}^-$  instead of  $\text{I}^-$  can be used as the top cell in tandem devices. Moreover, the capability of tuning the bandgap along all the visible range, with the appropriate ratio of halides, also makes the same materials extremely interesting for light emitting systems. Mixed halide perovskite materials are actively researched for solar cells with three main compounds  $\text{CH}_3\text{NH}_3\text{PbI}_3$ ,  $\text{CH}_3\text{NH}_3\text{PbBr}_3$  and  $\text{CH}_3\text{NH}_3\text{PbCl}_3$  showing little modifications in halide content (Nguyen et al., 2015). The direct band gap of semiconductors with a high absorption coefficient, a favorable band gap of 1.48-2.23 eV (Eperon et al., 2014; Noh et al., 2013). However, structural and electronic differences between the three materials, such as the definite role of I, Cl and Br anions have yet to be undoubtedly determined by the community. The scientist observed that incorporation of I or Cl as a dopant can improve the charge transport within the perovskites layer and increase the performance of the photovoltaic and optical properties. The Cl inclusion enhances the granular morphology resulting by electron beam induced current method (EBIC). These findings validate the band gap engineering strategies; the band gap of material might be efficiently adjusted by choosing the halide anion and the organic amide constituent. The

key aspects towards a low-coat technology capable of competing with the established silicon technology lies in the material low temperature solution process ability. The current method bare based on both one-step and two-step deposition of a mixture of  $PbX_2$  and  $CH_3NH_3I$  ( $X$  is halide anion) in a common solvent or sequential deposition of the constituents from a solution onto a mesoscopic scaffold and two-step coating methods. The coverage, pore-filling, and morphology of the deposited perovskite are found to be observed during coating. Both one-step and two step coating methods resulted in reproducible photovoltaic performance, but significant difference in especially photovoltage and fill factor. The electron life time was dependent on coating procedure (Im et al., 2014). Recent research has demonstrated an efficiency of 21.1% on mixing perovskite materials with inorganic cesium. This indicates that it is critical to have fine control over the nucleation and crystal growth of the  $MAPbI_3$ . The effort to control the morphology of the organometal trihalide perovskite based solar cell by varying processing conditions and the highest photocurrent are attainable only with the highest perovskite surface coverage (Saliba et al., 2016). As well known, despite the success in obtaining excellent photovoltaic performance, the instability of  $CH_3NH_3PbX_3$  to water and ambient moisture is still an open problem. Even though perovskite films have to be processed in inert atmosphere and devices cannot survive long in air, which hinder the production and applications of perovskite solar cells (Tai et al., 2016).

Even then, there are some caveats associated with the various components of the  $CH_3NH_3PbX_3$  based the stability of the absorber material in ambient conditions and the presence of toxic Pb to name a couple. Now research addressing these problems is being conducted worldwide through suitable replacements to both the  $CH_3NH_3$  and Pb

cations (Heo et al., 2014; Mitzi et al., 1995). The properties by changing the constituent elements give this class of material more scope of research and applicability. Such as the bandgap have been observed in the oxide perovskite in only a small variation in bandgap is in  $A\text{TiO}_3$  compounds, with A being Sr (3.57 eV), Ba (3.42 eV) and Pb (2.87eV) (Piskunov et al., 2004). However, there is a large change in bandgap on changing the B cation, e.g.  $\text{BaTiO}_3$  (3.72 eV) and  $\text{BaZrO}_3$  (5.04 eV) (Wang et al., 2014). The optimization of the absorber material in the case of the lead halide perovskites is also done in a similar manner, albeit via replacement of the halide i.e. I with Br and Cl and the associated changes in the band gap and structure was the subject of many studies (Yang et al., 2004; Wang et al., 2004; Fu et al., 2015; Nguyen et al., 2015). Similarly, reports on replacing or mixing organic A cation such as  $\text{CH}_3\text{NH}_3^+$  with formamidinium have shown that their stability in ambient conditions is increased, albeit its impact on properties of band gap (Noh et al., 2013).

In addition, during recent years a structurally hybrid perovskite architecture is essentially maintained. Today, this emerging field is largely driven by the intriguing properties of the hybrid perovskite  $\text{CH}_3\text{NH}_3\text{PbI}_3$  in thin film. However, other hybrid perovskite for example the family of perovskite like metal formats  $\text{AB}(\text{HCOO})_3$  (A= protonated amine, B= divalent metal), also show interesting properties such as multiferroic behavior and tunable mechanical properties (Kim et al., 2012; Liu et al., 2013; Im et al., 2011). From Goldschmidt's initial approach, effective ionic radii are used for calculating factors of hybrid perovskites. Goldschmidt's equation, factors are the effective ionic radius of the protonated amine A, the ionic radius of the anion X and the ionic radius of the divalent metal ion B in a perovskite with general formula  $\text{ABX}_3$ . The effective radii and heights of molecular anions were calculated according to

previous publication. Following the recent publication, the applied procedure and the ions used is given in Figure 2.7.

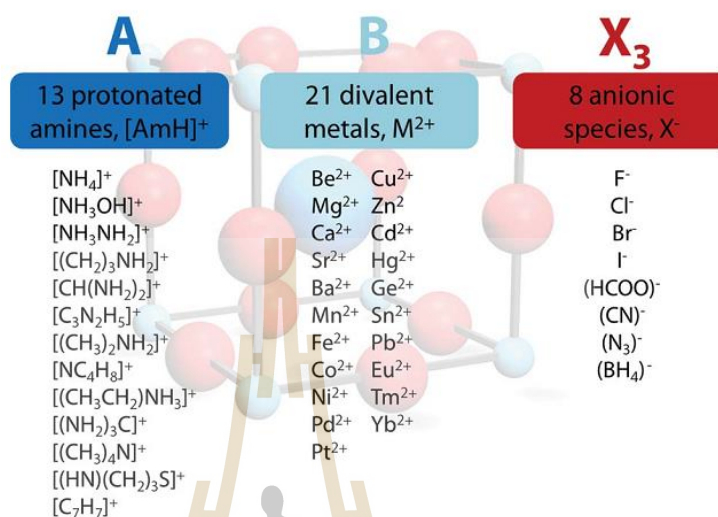
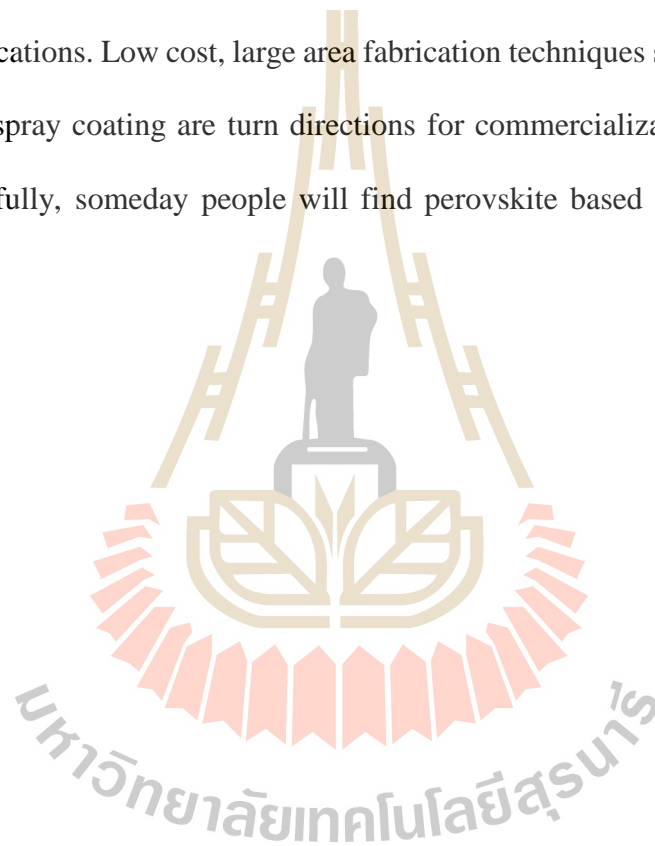


**Figure 2.7** Overview of the application procedure and the ions calculated 562 organic anion based, 180 halide (Kieslich et al., 2014).

Perovskite solar cells also find remarkable applications in water photolysis, photo-detectors and radiation sensing. They not only offer more complete photovoltaic technology but also provide a platform for the development of new photovoltaic materials and devices. In presently, trade solar cells working under encapsulation, so intrinsic instability (i.e., not due to the atmosphere surrounding the cells) is one of the key concerns, and the other one is the toxicity of Pb (Flora et al., 2012), which contains of the cells in a water soluble form. Some efforts have been paid to study stability. Good stability under full sunlight and high temperature was obtained for fully printable mesoscopic perovskite solar cells containing triple mesoporous layers (Lee et al., 2013). Replacing part of I<sup>-</sup> in CH<sub>3</sub>NH<sub>3</sub>PbI<sub>3</sub> with SCN<sup>-</sup> can greatly improve the moisture

tolerance of the resulting perovskite material. A crystal crosslinking tactically was applied to improve device stability. Device stability can be further improved by developing novel perovskite materials, highly efficient, stable and environmental friendly materials to replace current light absorbers could be found in the near future. Even though with defects but perovskite solar cells still show high potential for commercialization because of solution processing, low cost, very high efficiency and various applications. Low cost, large area fabrication techniques such as printing, blade coating and spray coating are turn directions for commercialization (Eslamian et al., 2014). Hopefully, someday people will find perovskite based on the product in the supermarket.



## **CHAPTER III**

### **RESEARCH METHODOLOGY**

In this chapter, the experimental procedures employed for preparation and characterization of the mixed halide perovskites powders will be describe the methods used in this thesis. Phase formation characterization has been carried out using x-ray diffraction (XRD) spectroscopy, simultaneous thermal analyzer (STA). Wide angle x-ray scattering (WAXS) was necessary to confirm the usual low angle structural parameters for our samples. Scanning electron microscopy (SEM) is used to investigate the surface morphology of the samples. After that x-ray fluorescence (XRF) was performed to determine the amount of Pb, I and Br using a sequential XRF spectrometer. We also performed uv-visible analyzes the light absorption of the perovskite structures and x-ray photoelectron spectroscopy (XPS) to examine the direct bandgap and survival of organic group of the elements within a material. The details of each experimental procedure will be described in the following sections.

#### **3.1 Sample preparation**

The main purposes of preparation methods are generally to create material of desired composition, which meets properties for good absorption properties.

##### **3.1.1 Powder preparation**

Methylammonium lead iodide mixing bromide powders used in this study were prepared using by a solid state mixed reaction technique. In the first step, we prepared

methylammonium iodide ( $\text{CH}_3\text{NH}_3\text{I}$  or MAI) by sol-gel technique between 12 mL hydroiodic acid (HI, 57 wt% in water, Aldrich) with 24 mL methylammonium ( $\text{CH}_3\text{NH}_2$ , 33 wt% in ethanol, Sigma Aldrich) in a 1:1 molar ratio. After the mixture was stirred continuously in the ice bath for 2 hours. Then, the solution was stirred at  $50^\circ\text{C}$  for 24 hours and  $\text{CH}_3\text{NH}_3\text{I}_3$  compound was obtained, the color of the dry product is light yellow. The resultant precipitates, in the form of white crystals to purify the salt. So, we can wash the dry product with diethyl ether (purity  $\geq 99.8\%$ , sigma aldrich) at room temperature to remove the residues, as the diethyl ether is a good solvent for amine and the acid but the salts have very low solubility in it. After washing the salts three times, a white powder (a little light yellow) could be obtained. The final  $\text{CH}_3\text{NH}_3\text{I}$  (MAI) ammonium salt is dried in vacuum oven at  $60^\circ\text{C}$  overnight.

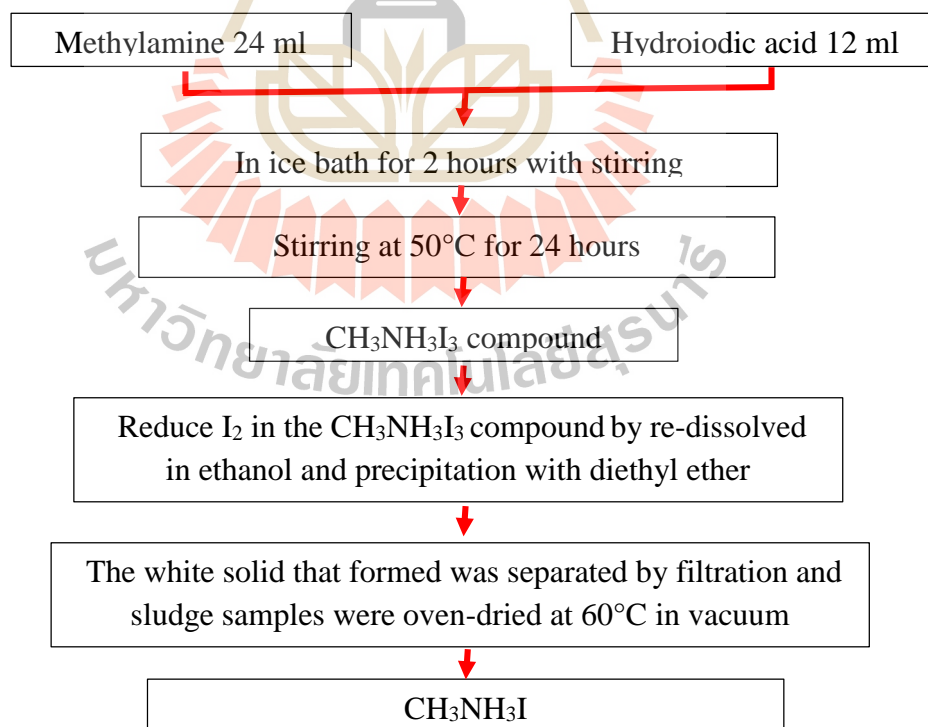


**Figure 3.1** Show the schematic diagram of the substrate  $\text{CH}_3\text{NH}_3\text{I}$  compound.

After the synthesis, the dry ammonium salts are used to prepare perovskite samples. In this stage, we introduce route to prepare the mixing-halide compound  $\text{CH}_3\text{NH}_3\text{PbIBr}_2$  was synthesized by solid-state reaction method, mixing 1:1 molar ratio of MAI to  $\text{PbBr}_2$  (purity 99%, sigma aldrich), ground with the mortar for a homogeneous for 30 minutes. The synthesis of  $\text{CH}_3\text{NH}_3\text{PbIBr}_2$  perovskite compound can be described by the following equation (1):



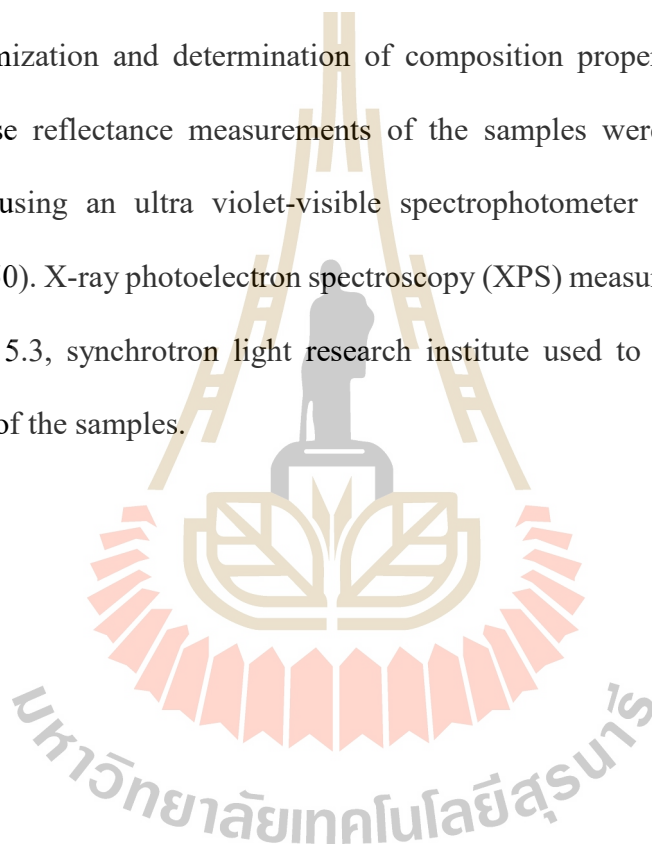
The as-prepared  $\text{CH}_3\text{NH}_3\text{PbIBr}_2$  was subsequently annealed in Ar for 30 minutes. The samples were annealed at different temperatures which were 150, 200, 225, 250, 275, 300 and 400°C.



**Figure 3.2** The sample powder of  $\text{CH}_3\text{NH}_3\text{PbIBr}_2$  perovskites.

In this study, the thermal properties of the perovskite compound can be checked by simultaneous thermal analyzer (STA). The phase formation, quality and crystalline

phase in the samples were investigated by x-ray diffraction (XRD) spectroscopy on a Bruker D8 Advance diffractometer using Cu-K $\alpha$  radiation and wide angle x-ray scattering (WAXS) technique was conducted on beamline 1.3, synchrotron light research institute to confirm the usual low angle structural. Wavelength dispersive x-ray fluorescence (ZXWD-XRF, Rigaku ZSXP rimus II) spectroscopy and scanning electron microscopy (SEM, FEI QUANTA 450) are a key complementary tool for process optimization and determination of composition property relationships. The optical diffuse reflectance measurements of the samples were performed at room temperature using an ultra violet-visible spectrophotometer (uv-vis, PerkinElmer LAMBDA 950). X-ray photoelectron spectroscopy (XPS) measurement was conducted on beamline 5.3, synchrotron light research institute used to analyze the chemical composition of the samples.



### 3.1.2 Research procedure

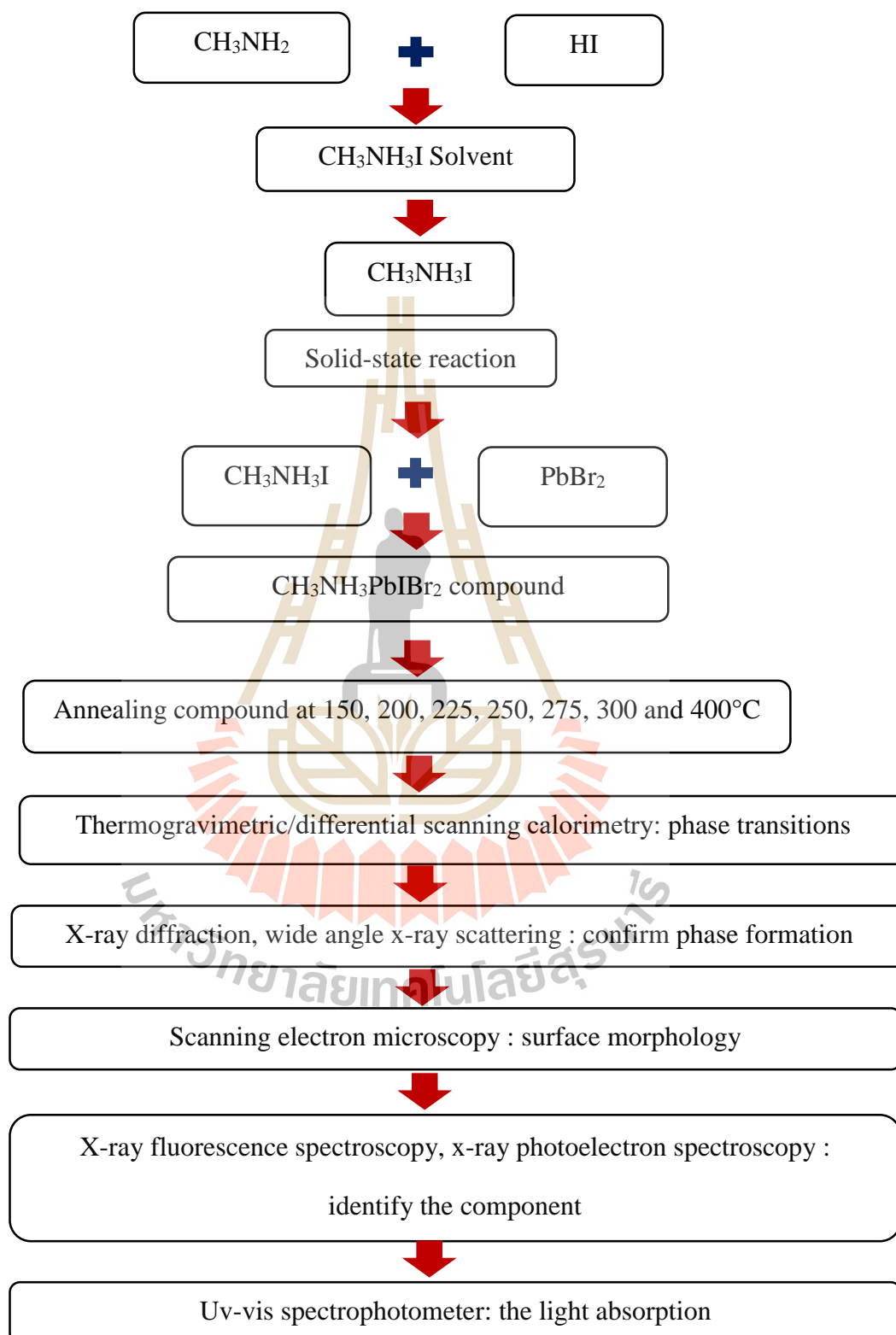


**Figure 3.3** Schematic diagrams for research procedure.

## 3.2 Sample characterizations

Characterization techniques used for subsequent investigation of phase formation, quality and crystalline phase, to confirm structure, optical properties and used to analyze the chemical composition of the samples.

### 3.2.1 Thermal analyzer

This work has been carried out using thermal analysis technique to study the effect of temperature in the composition of hybrid organic-inorganic perovskite products. The thermogravimetric analysis (TGA) and the differential scanning calorimetric (DSC) curves can also be used to analyse thermal stability decomposition of the perovskite compounds. So that the techniques can be used to determine annealing conditions and the consequent deterioration expected in the samples. By the simultaneous measurement of these two material properties not only improves productivity but also simplifies interpretation of the results. The complimentary information obtained allows differentiation between endothermic and exothermic events which have no associated weight loss (e.g. melting and crystallization) and those which involve a weight loss (e.g. degradation).

#### 3.2.1.1 Thermogravimetric analysis (TGA)

Thermo gravimetric analysis is a very useful technique to testing on samples which determines changes in weight to a temperature program in a controlled air. With this tool it is possible to characterize materials that exhibit weight loss or gain due to decomposition but as most weight loss curves look more or less similar, the weight loss curve may require keen analysis before results may be interpreted which a derivative weight loss curve can identify the point where weight loss is most prominent.

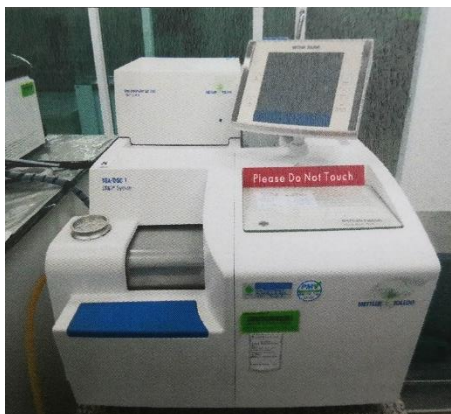


**Figure 3.4** Thermo gravimetric analyzer setting up at the center for scientific and technological equipment.

### 3.2.1.2 Differential scanning calorimetry technique (DSC)

Differential scanning calorimetry technique is the most widely used a method in characterization of material research that is employed to measure the heat effects of phase transitions of a sample material. DSC is used to identify phase transitions such as glass transition, crystallization and decomposition. We are interested to find phase transformations of a material are accompanied by exothermic or endothermic reactions.



**Figure 3.5** Differential scanning calorimetry setting up at the center for scientific and technological equipment.

### 3.2.2 X-ray diffraction (XRD) technique

The x-ray diffraction measure was used to analyze phase formation of the perovskites in  $\text{CH}_3\text{NH}_3\text{PbI}\text{Br}_2$  system. Room temperature XRD patterns were recorded between  $2\theta = 0^\circ$  to  $50^\circ$ . A Bruker D8 Advance diffractometer using  $\text{Cu-K}\alpha$  radiation as shown in Figure 3.6.



**Figure 3.6** X-ray diffraction (XRD) setting up at the center for scientific and technological equipment.

The x-ray diffraction measure is a multifunction, non-destructive analytical technique for examples bulk materials, thin films and powders. It provides information on crystal structure, phase, preferred crystal orientation (texture), the chemical composition, crystallographic structure and other structural parameters such as crystallinity, strain, and crystal defects. This is a useful tool when trying to positively identify a contaminant or corrosion product and for identification of foreign phases for purity analyses of crystalline materials (e.g. organic, minerals, inorganic compounds). X-ray diffraction is based on constructive interference of monochromatic x-rays and a crystalline sample. These x-rays are generated by a cathode ray tube, filtered to produce

monochromatic radiation, collimated to concentrate and directed toward the sample. Which the result from an XRD analysis is a diffractogram showing the intensity as a function of the diffraction angles. Also the peak intensities are determined by the distribution of atoms within the lattice. Consequently, the x-ray diffraction pattern is the fingerprint of the periodic atomic arrangements in a given material. The principle of x-ray diffraction is characterized by Bragg's law of reflection can be described by the following equation (2).

$$2d \sin\theta = n\lambda \quad (2)$$

Where  $n$  is the number of atom layers,  $\lambda$  is the wavelength of the used x-rays,  $d$  is the lattice plane spacing of a family of crystallographic planes (hkl) responsible for the Bragg peak,  $\theta$  is the angular position of this diffraction peak.

The Bragg's condition for constructive interference results in only some angles being strong enough for detection. In the Figure 3.7 shows the schematic representation of XRD characterization principle.

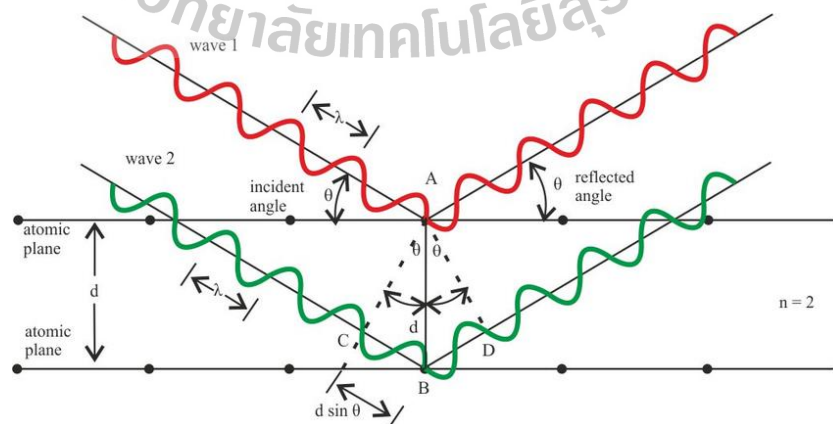


**Figure 3.7** The schematic representation of XRD characterization principle.

### 3.2.3 Wide-angle x-ray scattering technique

The x-ray scattering has been widely used in the study of density domains from a tenth to a thousandth angstrom. Essentially, x-ray scattering techniques also show a major role in obtaining information of both the structure and morphology of materials in the nano-systems. This range of domain size requires the wide-angle x-ray scattering technique (WAXS), roughly this technique covers from 1 nm down and possibly 100 nm for a finely tuned tool. WAXS is a powerful technique in giving about information on the crystallographic structure, chemical compositions and as well as chemical stoichiometry. The experiments were performed in the joint wide-angle x-ray scattering technique (WAXS) at Synchrotron Thailand on beam line 1.3. The data processing program called SAXSIT which is developed in-house is also available to process the 2D scattering pattern. The program SAXSIT has been developed by BL1.3W team for processing of scattering patterns, data manipulation and some fitting and modeling.



**Figure 3.8** WAXS experimental which BL1.3 set up at synchrotron light research institute.

### 3.2.4 Scanning electron microscopy (SEM)

Scanning electron microscopy (SEM) is used to investigate the surface morphology of the samples. SEM has high resolution ( $\sim 1$  nm) and it is used to image and characterize small-scale details. The scanning electron microscope focuses an electron beam to the surface of the sample. The electrons interact with the surface resulting for example secondary electrons and back-scattered electrons. So, the electrons are detected to produce images. Average particle size of the perovskites compound were estimated by using a linear intercept method, where random line were drawn on a micrograph and the number of particle intercepting these line were then counted. FEI QUANTA 450 scanning electron microscope was used for this study shown in Figure 3.9.



**Figure 3.9** Scanning electron microscopy (SEM) used in this study.

### 3.2.5 X-ray fluorescence spectroscopy (XRF)

X-ray fluorescence (XRF) spectrometry is an elemental analysis technique with wide application in many industries and scientific fields. One has to consider that XRF

is a surface-sensitive method because of the energy of the excited and emitted radiation which is in the range 1–115 keV (Be to U K-radiation). XRF is based on the principle that individual atoms, when excited by an external energy source, emit X-ray photons of a characteristic wavelength. By counting the number of photons of each energy emitted from a sample, the elements present may be identified and quantitated.



**Figure 3.10** X-ray fluorescence spectroscopy.

### **3.2.6 Uv-vis spectrophotometer technique**

The measurement of the band gap of materials is very important in the semiconductor, nanomaterial and solar industries. Which a measuring the band gap of a material can be determined from its uv-vis absorption spectrum. The band gap refers to the energy difference between valence band and conduction band which is measured in eV. By the wide of this band gap gives the materials some of their distinct properties. In several papers, I found that the optimized band gap for solar cells is close to 1.5 eV, the value corresponds to a wavelength of about 827 nm. In the part of semiconductors, incident photons with higher energies than the band gap energy excite an electron while

the ones with lower energies are transmitted. The absorption coefficient of the samples was calculated by using the Tauc relation. A Tauc plot is used to determine the optical bandgap in semiconductors. Tauc gap is often used to characterize practical optical properties of materials. The band gap of the material can be found by intersecting the plot with x-axis. The equation of this plot is given as;

$$\alpha hv = A(hv - E_g)^n \quad (3)$$

where  $\alpha$  is the absorption coefficient,  $hv$  is energy of the incident photon,  $E_g$  is bandgap and  $A$  is a constant. The superscript  $n$  is dependent on the material type. For direct band gap materials, it is 0.5. To determine the band gap, the Tauc plot is linearly intersected to the x-axis from the optical band edge value.



**Figure 3.11** Uv-vis spectrophotometer experimental at synchrotron light research institute.

### 3.2.7 X-ray photoelectron spectroscopy technique

X-ray photoelectron spectroscopy (XPS) is a quantitative spectroscopic technique that can be used to examine the elemental composition of a material as well as the chemical and electronic state of the elements, to probe the changes that occur at the interface and to elucidate the electron transport mechanisms, x-ray photoelectron spectroscopy was conducted and the core-level spectra was investigated. As the demand for high performance materials increases, so does the importance of surface engineering. Many of the problems associated with modern materials can only be solved by better understanding the physical and chemical interactions that occur at the surface or at the interfaces of a material's layers. In the part of sample is irradiated by a beam of x-rays, which cause core electrons to be ejected from the sample surface. A spectrum of the energies of these ejected electrons is recorded. The electron energies of interest usually lie in the range of 0-1500 eV, since the escape depth of electrons at these energies is typically between 2 and 8 monolayers, XPS is surface specific (in the top 1-10 nm of the sample). The identification of individual species and their elemental and chemical states are based on the fact that the emitted electron have a characteristic binding energy (BE), corresponding to the atom's electron shell structure (1s, 2s, 2p, 3p etc). The binding energy of an electron is characteristic of the elemental core energy level from which it was emitted, so XPS is a useful tool for determining the elemental composition of a surface. In this work, the spectra were recorded at pressure to measure C, N, O, Pb, I and Br elements.

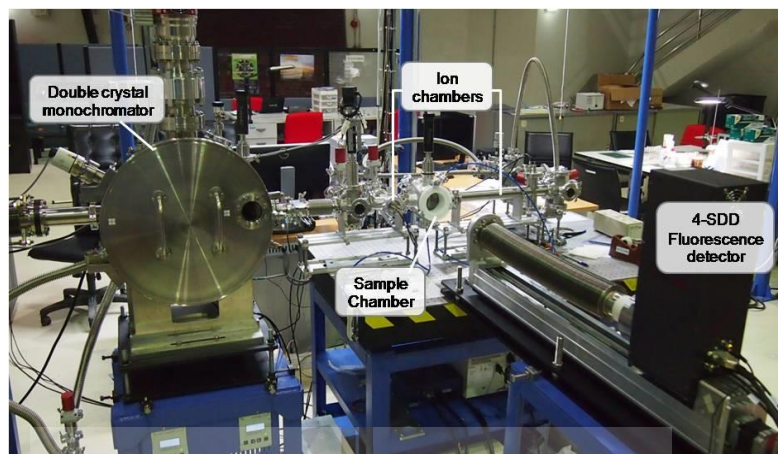
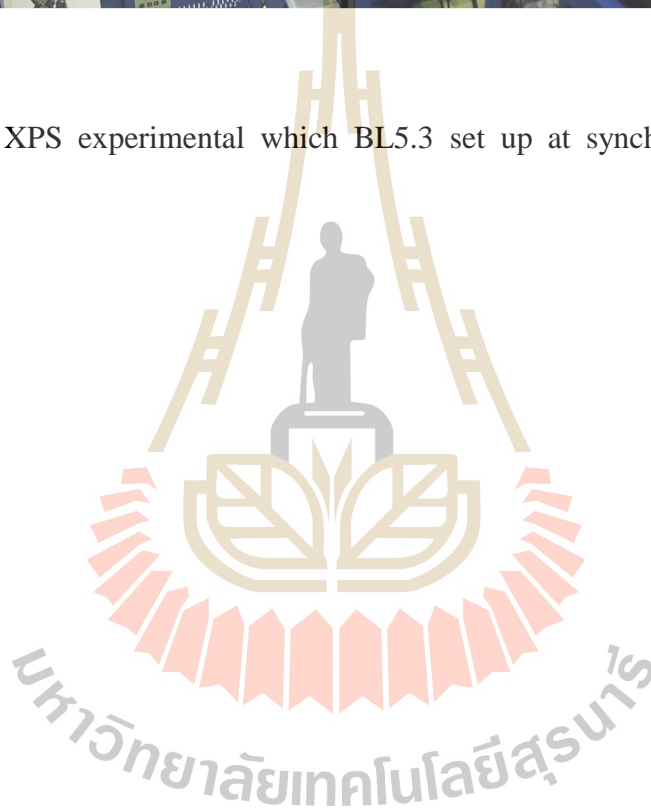


**Figure 3.12** XPS experimental which BL5.3 set up at synchrotron light research institute.



## **CHAPTER IV**

### **RESULTS AND DISSCUSSION**

In this chapter, the result of the mixed bromide iodide lead perovskites compound ( $\text{CH}_3\text{NH}_3\text{PbIBr}_2$ ) were analyzed and discussed in the powder forms. The motivation of this study is to tune the band gap and improve term stability of mixed halide perovskites by solid state reaction method. The annealing temperature condition parameters were changed and their effects on the properties are demonstrated. Absorption, band gap, structure, phase formation and the optical properties of bromide-iodide mixed lead perovskite powder will be explained and discussed.

#### **4.1 Simultaneous thermal analysis (STA)**

Thermogravimetric analysis was used for imposing the mass loss behavior of the individual organic and inorganic components that make up the building blocks of  $\text{CH}_3\text{NH}_3\text{PbIBr}_2$  as a function of annealing temperature. Considering thermal stability which is also an important property for halide perovskites for the new applications, we carried out thermogravimetric and differential scanning calorimetry analysis of the as-prepared  $\text{CH}_3\text{NH}_3\text{PbIBr}_2$  powder sample. The sublimation behavior of the separated organic-inorganic component was examined in depth and used to interpret the TGA data of the  $\text{CH}_3\text{NH}_3\text{I}$  salt,  $\text{CH}_3\text{NH}_3\text{PbIBr}_2$  powder and  $\text{PbBr}_2$  compound. A significant difference between the compounds was observed in terms of thermal stability.

Hence, some researchers focused on the preparation of mixed halide perovskite, the substitution of iodine by bromide atoms leads to a significant improvement of perovskite stability. Although, there are many studies on the growth of mixed halide bromine perovskite, their formation process remains poorly investigated. Figure 4.1 shows a higher degradation onset temperature of  $\text{CH}_3\text{NH}_3\text{PbIBr}_2$  (first onset at  $\sim 200^\circ\text{C}$ ) than of  $\text{CH}_3\text{NH}_3\text{I}$  (first onset at  $\sim 150^\circ\text{C}$ ) and the inorganic compound of  $\text{PbBr}_2$  onset at  $\sim 400^\circ\text{C}$ .

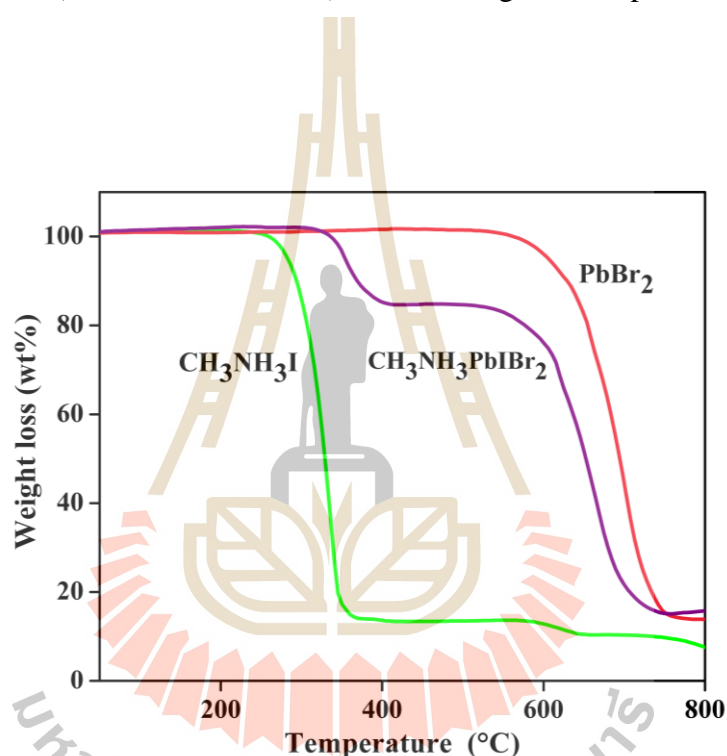


**Figure 4.1** Thermogravimetric analyses of methylammonium iodide ( $\text{CH}_3\text{NH}_3\text{I}$ ), methylammonium lead iodide-bromide ( $\text{CH}_3\text{NH}_3\text{PbIBr}_2$ ) and lead bromide ( $\text{PbBr}_2$ ), showing the higher thermal stability of the inorganic perovskite compared to the hybrid organic-inorganic perovskite.

The degradation process of methylammonium lead iodide-bromide samples can be subdivided into three stages based on TGA curves. The first step centered at around

150°C with the small weight loss is assumed to be the release of adsorbed water from the sample. Furthermore, the next step mass loss is 15 wt%, ascribed to the nominal loss of methylammonium iodide, by the onset of which occurs at 150°C suggesting the sublimation of these materials, which mainly occurred from 300 to 430°C. In this case, the obvious exothermic peak shown on the DSC result is centered at about 360°C, which is connected to the evaporation of methylammonium halides. A possibility that had to be taken into account considers that all the methylammonium halides under consideration have melting points over 200°C. Finally, the third mass loss of 69 wt%, the large mass loss profile seen in the TGA first derivative implies that these inorganic materials undergo thermal decomposition between 420 and 700°C for sample in good agreement with the thermal decomposition of the inorganic  $\text{PbBr}_2$  proportion of the perovskite formed and centered at around 635°C. Meanwhile, the differential scanning calorimetry (DSC) analysis was used to measure phase transition of the composites. The results indicate that methylammonium lead iodide-bromide ( $\text{CH}_3\text{NH}_3\text{PbIBr}_2$ ) is relatively stable at about 250°C. It can be seen by sharp transition stage in the temperature range DSC peak at 150°C and 350°C, Figure 4.2 DSC curve shows three endothermic peaks in the temperature ranges 150-165°C, 310-400°C, and 410-790°C. The endotherm peak on the DSC curve is conducted for the purpose of evaluating the physical and chemical changes that may take place in a sample as a result of thermally induced endothermic reactions. After that, some obvious decomposition reaction occurs enabling the materials to lose functionality completely. In the temperature range demonstrated that around 310-400°C, may be assumed that sample has phase formation around lower endotherm and higher endotherm has phase transform. Above 400°C, TGA curve indicates that higher mass loss of substance occurs. This TGA and DSC

results imply the upper limit of the annealing temperature for the mixed powders. Therefore, the temperature used to define the range of annealing temperature (150-400°C) used in subsequent powder processing steps.

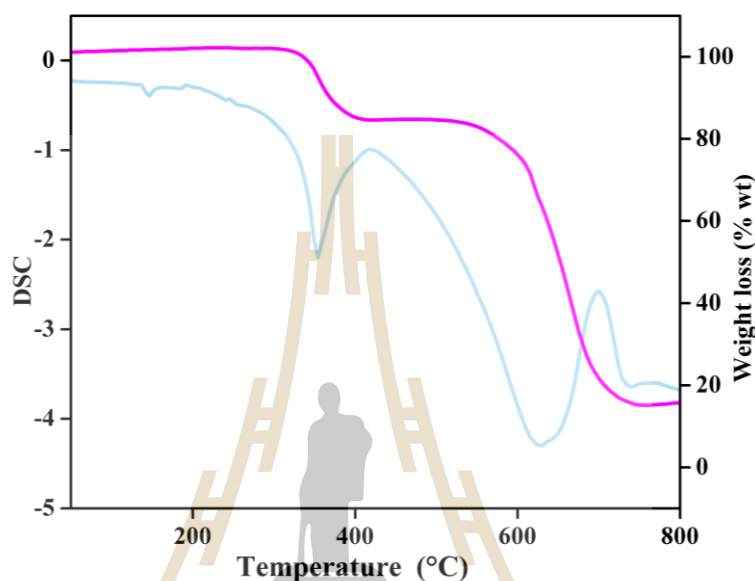


**Figure 4.2** TGA heating curves of individual precursor powders expressed as weight % as a function of applied temperature and the corresponding first derivatives.

#### 4.1.1 Goldschmidt's tolerance factor

The tolerance factor ( $t$ ) is a largely used predictor of perovskite stability. The freshly, attention in hybrid perovskites for use as solar cell absorbers has leads to many applications of the tolerance factor to these materials are the way to explain and predict structure. So, we critically assess the suitability of the tolerance factor for halide perovskites. The general chemical formula of hybrid perovskites is  $ABX_3$ , where A is monovalent organic cation: methylammonium iodide  $MA^+$  and  $Pb^+$ , B is divalent metal cation and X is halide anion such as  $Br^-$ ,  $I^-$  or their mixtures. Goldschmidt tolerance

factor is a reliable empirical index to predict which stable crystal structures of perovskite materials, which can be calculated from the ionic radius of the atoms can be estimated by equations (1):

$$t = \frac{R_A + R_X}{\sqrt{2}(R_B + R_X)} \quad (1)$$

where  $R_A$  and  $R_B$  are the ionic radius of the A and B site cations respectively, and  $R_X$  is the ionic radius of the anion.

**Table 4.1** Ionic radii is used for calculating tolerance factor of hybrid perovskite.

| Ion               | A Cation | B Cation | X Anion |     |
|-------------------|----------|----------|---------|-----|
|                   | MA       | Pb       | I       | Br  |
| Ionic radius (pm) | 217      | 119      | 220     | 196 |

If a tolerance factor of 1 indicates the ideal cubic structures form  $t$ ; in the range  $0.8 \leq t \leq 1$  perovskites generally do form. Lower values of  $t$  will lower the symmetry of the crystal structure. When we calculate the tolerance factors value lies in the range of 0.89 – 0.94, cubic perovskite structures with high stability are formed. Since perovskites are not truly ionic compounds and since the  $t$  values also depend on what values are taken for the ionic radii, the tolerance factor is only a rough estimate.

## 4.2 Phase formation by X-ray diffraction (XRD)

X-ray diffraction (XRD) measurement was then employed to determine the conditions of thermal annealing on the formation phases and crystallization in the above 8 different samples were labeled for comparison with the calculated XRD data using X'pert high score plus software. The structural information of the intermediate and phase transition was collected using x-ray diffraction measurements as shown in Figure 4.3. The effect of the annealing temperature on the preparation of mixed halide perovskite compound prepared using the solid-state reaction technique was studied by Wang (Wang et al., 2014). Earlier study by Li (Li et al., 2013) also shown similar observation. It reveals that the annealing temperature at 150°C for 30 min has negligible influence on CH<sub>3</sub>NH<sub>3</sub>PbIBr<sub>2</sub> structures. Instead, dramatic changes in crystal structure occur when the annealing temperature increases to 200°C due to the decomposition of CH<sub>3</sub>NH<sub>3</sub>I (Dualeh et al., 2014). In this works presented the diffraction patterns of CH<sub>3</sub>NH<sub>3</sub>PbIBr<sub>2</sub> compounds annealed at 150, 200, 225, 250, 300 and 400°C for 30 min, the peak intensity indicates the formation of perovskite phases and secondary phases related to the dopants are detected with can be matched with JCPDS file 00-031-0679 for orthorhombic phase of PbBr<sub>2</sub> and JCPDS file no 00-010-0737 for tetragonal phase of CH<sub>3</sub>NH<sub>3</sub>I or MAI. Some other interesting peaks observed are the ones at  $2\theta = 12.3^\circ, 14.7^\circ, 28.2^\circ$  and  $33.1^\circ$  could correspond to the (101), (111), (212), (310) planes of the perovskite crystalline structure, respectively. Due to the XRD result also indicates that the increase of the annealing temperature causes a gradual shift in diffraction peaks toward lower angles, suggesting larger lattice parameter. Due to the slight excess of lead bromide, there is another strong Bragg diffraction peak at  $2\theta = 14.6^\circ$ , which could be attributed to the (111) face of PbBr<sub>2</sub>. Also peaks seem to be

slightly shifted towards  $14.6^\circ$  which imply that the particle becomes more crystallized as the annealing temperature increases. The original of  $\text{CH}_3\text{NH}_3\text{PbIBr}_2$  crystalized in a tetragonal structure (Priyabrata et al., 2015) with a space group of  $I4/mcm$ . The lattice parameters of  $a = b = 8.4822 \text{ \AA}$  and  $c = 11.9944 \text{ \AA}$  are indexed using ICSD 4124388.

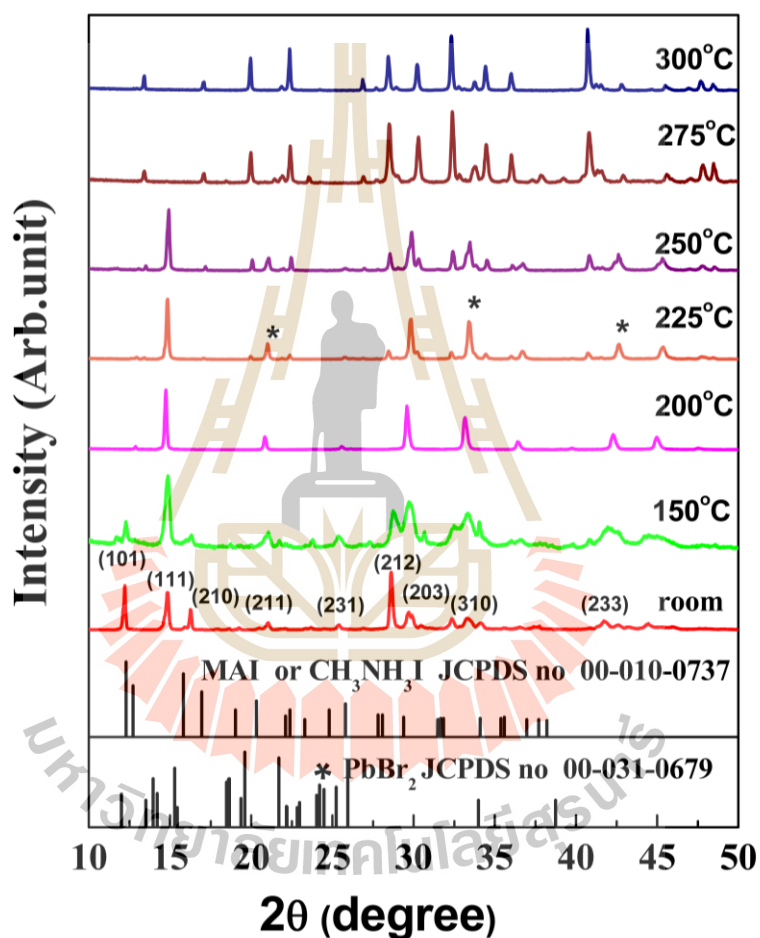


**Figure 4.3** The XRD patterns for the samples synthesized,  $\text{CH}_3\text{NH}_3\text{PbIBr}_2$ .

The intensity of  $\text{CH}_3\text{NH}_3\text{PbIBr}_2$  characteristic peaks gradually raised with reduced full width at half maximum when annealing temperature is increased along with few peaks disappeared and new minor peaks appear at 200°C due to elimination

of defects. It can be noticed the Figure 4.3, the magnification of (212) and (310) peak as the temperature increases, the (310) peak gradually decrease and the height of the (212) peak increases. As the iodine atoms are gradually substituted with the smaller bromine atoms, the tetragonal phase is gradually transited to the cubic phase. We can see that the main perovskite diffraction peaks are significantly enhanced with the increase of the annealing temperature from 150 to 250°C, indicating an improvement of peak at 14.6° corresponding to cubic structure. However, the sharp peak for the perovskite samples presents the high crystallinity of the powders. Due to the annealed samples exhibit cubic (Samapti et al., 2014) structure and larger cell parameter by rietveld refinement, the average crystallite size was calculated by using the scherrer equation.

$$D = \frac{k\lambda}{\beta \cos \theta} \quad (2)$$

Where D is average crystallite size,  $\lambda$  is wavelength (1.5406 Å), k is a dimensionless shape factor = 0.89;  $\theta$  is the Bragg's diffraction angle of the planes in degrees and  $\beta$  is the corrected full width at half-maximum (FWHM) of XRD patterns.

The above x-ray powder diffraction patterns are performed at the wavelength of 1.54 Å with a step size of 0.02° from 10° to 50° of 2 $\theta$  range. At high annealing temperatures, both the lattice parameters and the crystallinity increased as a consequence of incomplete conversion of CH<sub>3</sub>NH<sub>3</sub>I + PbBr<sub>2</sub> into the perovskite phase also resulting in appearance of the secondary phases. At higher temperature (225°C) a

more complete phase formation was observed, as confirmed by Rietveld refinement. But we could not achieve complete phase purity of the  $\text{CH}_3\text{NH}_3\text{PbIBr}_2$  perovskite.

In addition to the main phase, the peak at  $2\theta = 14.6^\circ$  originating from  $\text{PbBr}_2$  was present in all the samples both annealed and as-prepared. This is consistent with the results reported in reference (Prasenjit et al., 2015). However, our results show that annealing at  $225^\circ\text{C}$  can significantly suppress the  $\text{PbBr}_2$  secondary phase in our powder down to 3.74%.

**Table 4.2** The crystallographic structural data of  $\text{CH}_3\text{NH}_3\text{PbIBr}_2$  diffraction peak of full width at half-maximum (FWHM) and crystallite size by Rietveld refinement of the XRD pattern.

| Sample   | %Phase formation                       |                 | FWHM   | Crystallite size (nm) |
|--|--|-----------------|--------|-----------------------|
|  | $\text{CH}_3\text{NH}_3\text{PbIBr}_2$ | $\text{PbBr}_2$ |        |                       |
| $\text{CH}_3\text{NH}_3\text{PbIBr}_2_{\text{room}}$       | 46.62                                  | 53.38           | 0.1378 | 56.19                 |
| $\text{CH}_3\text{NH}_3\text{PbIBr}_2_{150^\circ\text{C}}$ | 73.48                                  | 26.52           | 0.1378 | 56.80                 |
| $\text{CH}_3\text{NH}_3\text{PbIBr}_2_{200^\circ\text{C}}$ | 93.44                                  | 6.56            | 0.1181 | 65.39                 |
| $\text{CH}_3\text{NH}_3\text{PbIBr}_2_{225^\circ\text{C}}$ | 96.26                                  | 3.74            | 0.1181 | 67.69                 |
| $\text{CH}_3\text{NH}_3\text{PbIBr}_2_{250^\circ\text{C}}$ | 93.57                                  | 6.43            | 0.0984 | 78.69                 |

According to the full width at half-maximum (FWHM) values, the crystallite size of the perovskite powder could be estimated in terms of the Scherrer equation to be

around 50 and 80 nm for samples with annealing temperature conditions of room, 150, 200, 225 and 250°C samples.

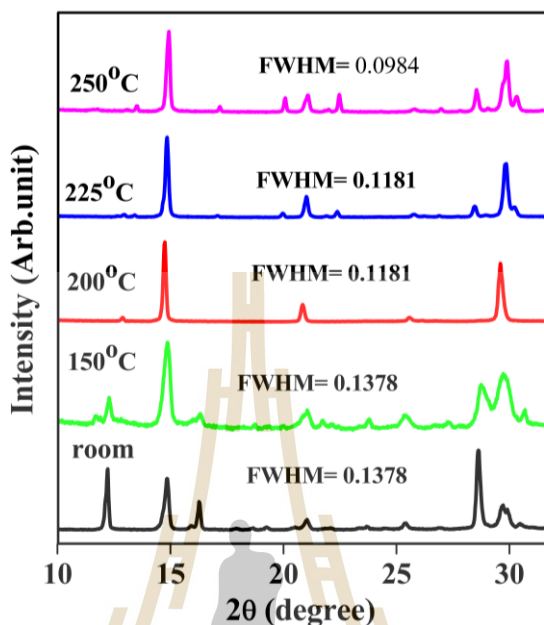


**Figure 4.4** The XRD patterns present the diffraction peak of full width at half-maximum (FWHM).

Therefore, the particle size of each sample was determined from the x-ray data using Scherer's formula. The effect of particle size with increase in annealing temperature has been shown in Figure 4.4. In annealing process when the particles are formed, they collide and either coalesce with one another to form a larger particle or coagulate. The process which occurs depends upon the temperature and available energy, that's why particle size increases with increasing temperature. When the sample amount, sample powder is smaller, it is difficult to obtain the necessary diffraction amplitude by XRD. Since the amount is enough for the SEM observation, only SEM observation may be applied to obtain the structure data.

### 4.3 Scanning electron microscopy (SEM)

Scanning electron microscopy results, discussion of the use of SEM as a primary tool for the characterization of particle size, distributions is presented. SEM images of the  $\text{CH}_3\text{NH}_3\text{PbIBr}_2$  compounds are shown in Figure 4.5, illustrating the corresponding morphological in the compound under the annealing temperature condition. Different annealing conditions result in different morphology of the  $\text{CH}_3\text{NH}_3\text{PbIBr}_2$  compounds. The average particle size, for sample is from 40 to 80  $\mu\text{m}$ , with increasing temperature condition of the perovskite compound from 150 to 250°C. It further indicates that the particle size increases with increasing annealing temperature.

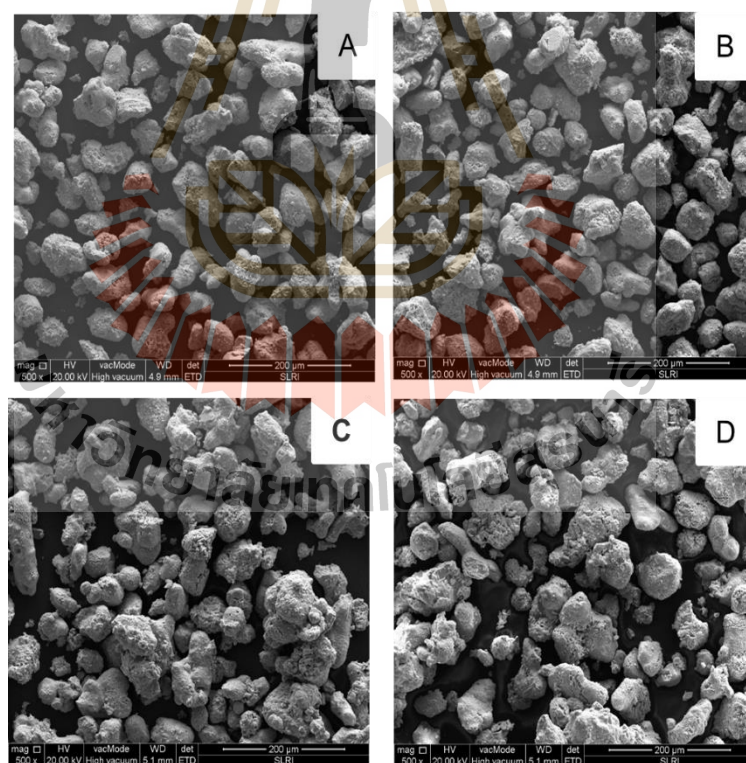


**Figure 4.5** SEM images of  $\text{CH}_3\text{NH}_3\text{PbIBr}_2$  compounds thermally annealed at various temperatures at (A) 150°C, (B) 200°C, (C) 225°C, (D) 250°C.

**Table 4.3** The particle size of  $\text{CH}_3\text{NH}_3\text{PbIBr}_2$ .

| Annealing temperature (°C) | Time (second) | Particle size range (nm) |
|----------------------------|---------------|--------------------------|
| 150                        | 30            | $40 \pm 1$               |
| 200                        | 30            | $60 \pm 1$               |
| 225                        | 30            | $73 \pm 1$               |
| 250                        | 30            | $82 \pm 1$               |

#### 4.4 Wide angle x-ray scattering (WAXS)

Wide-angle x-ray scattering (WAXS) is often used to determine the crystalline structure of compound. To better understand the enhancement in charge transport with increasing particle size, we performed XRD crystallography analysis on the samples. In Figure 4.6, we compare wide-angle x-ray scattering (WAXS) images of samples prepared with different the annealing temperature of precursor. Furthermore, it is apparently from the XRD that results with larger particle size show significant sharper diffraction spots than those with small size. Detailed structural analysis of the thermal annealing on the formation of perovskite phases by high-resolution WAXS presented strong peaks at  $2\theta = 14.51^\circ$ ,  $29.7^\circ$  and  $33.2^\circ$  are clearly visible which can be respectively indexed as (111), (212) and (310) planes in tetragonal structure with a space group of  $I4/mcm$  phase. Moreover, WAXS result shown the  $\text{CH}_3\text{NH}_3\text{PbIBr}_2$  compounds were thermally stable the compounds an annealed at  $150^\circ\text{C}$  and  $225^\circ\text{C}$  did not show dramatic changes in their WAXS patterns compared with the annealed at  $150^\circ\text{C}$  and  $225^\circ\text{C}$  from XRD results. This indicates that the samples of annealed at

225°C for 30 min was not completely decomposed into  $\text{PbBr}_2$ , this change confirms that the decomposition of  $\text{CH}_3\text{NH}_3\text{PbIBr}_2$  was completed by annealing at 250°C for 30 min. The thermal decomposition in the temperature range from  $\sim 250^\circ\text{C}$  involves the formation of structural changes in the remaining crystalline phase.

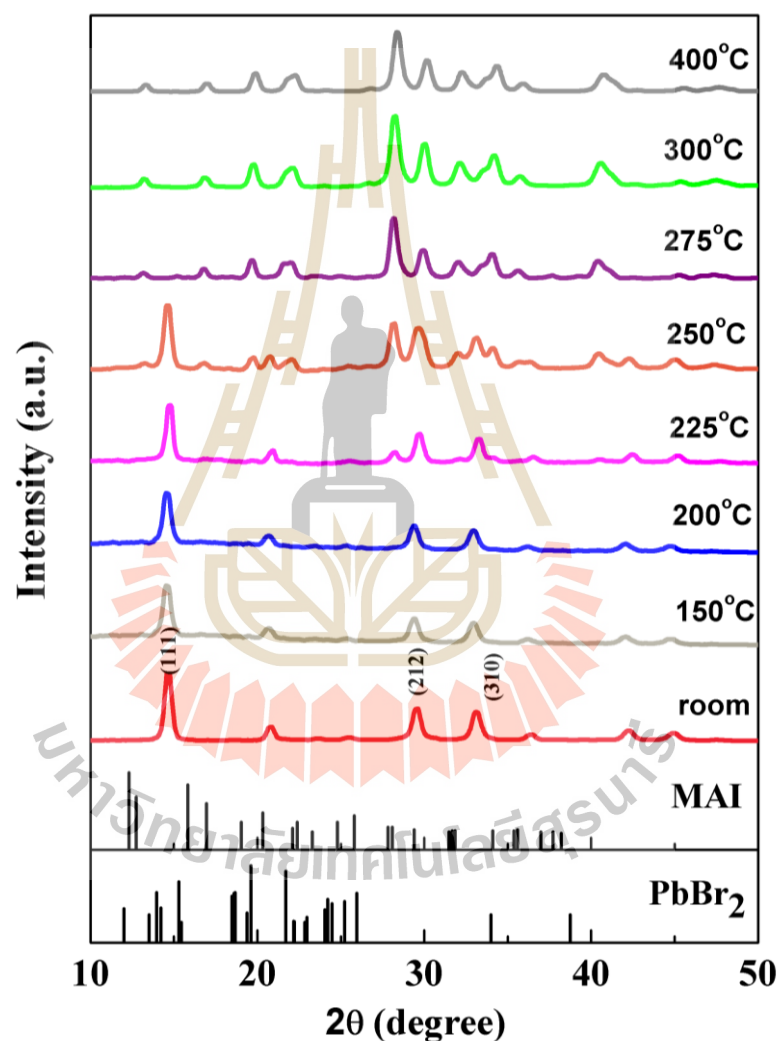


**Figure 4.6** WAXS images of  $\text{CH}_3\text{NH}_3\text{PbIBr}_2$  compounds and annealed samples at various temperatures.

#### 4.5 X-ray Fluorescence spectroscopy (XRF)

The elemental analysis of the synthesized samples was performed using XRF to determine the amount of Pb, I and Br the dopant incorporated into the structure and with the XRF technique to detect the amount of Pb, I and Br. The weight percentages of each of the elements in the synthesized samples were obtained the atomic percentages were determined in Table 4.4.

**Table 4.4** Weight percentage values for the elements in the samples prepared, obtained by means of XRF technique.

| Weight percentage | Sample   |   | lines  |
|-------------------|--|---|--------|
|                   | CH <sub>3</sub> NH <sub>3</sub> PbIBr <sub>2</sub> _room | CH <sub>3</sub> NH <sub>3</sub> PbIBr <sub>2</sub> _225 |        |
| Pb                | 41.3 ± 0.1   | 43.0 ± 0.1  | Pb-Lβ1 |
| I                 | 28.3 ± 0.1   | 26.5 ± 0.1  | I-Kα   |
| Br                | 31.4 ± 0.1   | 30.5 ± 0.1  | Br-Kα  |

The results of the weight percentages obtained are shown in Table 4.4, which also shows the atomic percentage calculated for each element. It is possible to observe only small deviations with regard to the nominal composition. To enhance understanding, in the discussion of the results the CH<sub>3</sub>NH<sub>3</sub>PbI<sub>x</sub>Br<sub>3-x</sub> will be identified by the nominal value of x = 1. In addition, the atomic ratios of the CH<sub>3</sub>NH<sub>3</sub>PbI<sub>x</sub>Br<sub>3-x</sub> as-prepared and as-annealed at various annealing temperatures (225°C) are Pb:I:Br = 1: 1: 2 and Pb:

I:Br = 1: 1: 2 for  $\text{CH}_3\text{NH}_3\text{PbIBr}_2$  and  $\text{CH}_3\text{NH}_3\text{PbIBr}_{2\_225}$ , which is stoichiometric value.

#### 4.6 Uv-vis spectrophotometer

We explore the impact of the temperature of crystallization upon the optical properties of crystals. It is well known that the ability of the halide anion to tune the bandgap of the corresponding perovskite crystals depends on their temperature where halide group of perovskites show the bandgap ( $E_g$ ). On the other hand, some researchers have found that  $\text{MAPbI}_3$  is more sensitive to moisture and humidity than  $\text{MAPbBr}_3$  but the absorption of  $\text{MAPbBr}_3$  is not comparable to that of  $\text{MAPbI}_3$ . Hence, we focused on the preparation of mixed halide perovskite  $\text{CH}_3\text{NH}_3\text{PbIBr}_2$  compounds. Changing the annealing temperature fraction contained in  $\text{CH}_3\text{NH}_3\text{PbIBr}_2$  compounds affects the optical properties of the perovskites compound. Figure 4.7 present the uv-vis absorbance spectrum of the samples with various annealing temperature. It was observed that increasing the annealing temperature of methylammonium lead iodide bromide samples introduced to the absorption onset gradually shifts to the lower photon energy (to shorter wavelength of light), indicating the increase of the band gap energy of the prepared perovskites compound. The band gap is calculated using by Kubelka-Munk (K-M) function to the measured diffused reflectance spectra. The K-M function,  $(F(R))$  was calculated by extrapolating a straight line to the  $(F(R)hv)^2$  axis in the plots of the  $(F(R)hv)^2$  versus optical band gap energy, used for the Tauc plots were plotted against photon energy. The Tauc plot is a method that is widely used for the determination of band gap from a diffuse reflectance spectrum (in the Table 4.5).

Experimentally, we can get the value of  $E_g$  by usually use the Tauc relation, which is given by this equation:

$$[F(R)hv]^n = A (hv - E_g)$$

where  $\alpha$  is absorption coefficient given by

$$F(R) = \alpha = \frac{(\ln(1-R))^2}{T}$$

where T and R are the transmission and reflection, while (hv) is the photon energy.

$$hv \text{ (eV.)} = \frac{1240}{\text{incident wavelength(nm.)}}$$

According to the literature, the optical absorption for this kind of perovskite occurs via direct transition. So, the optical band gap  $E_g$  was determined from the extrapolation of the linear part of the  $[F(R)hv]^2$  vs  $hv$  plot, the values found are shown in Table 4.5.

**Table 4.5** The data band gap of samples.

| Sample  | Band gap (eV.) |
|---|----------------|
| CH <sub>3</sub> NH <sub>3</sub> PbIBr <sub>2</sub> _room  | 1.890 ± 0.002  |
| CH <sub>3</sub> NH <sub>3</sub> PbIBr <sub>2</sub> _150°C | 1.840 ± 0.003  |
| CH <sub>3</sub> NH <sub>3</sub> PbIBr <sub>2</sub> _200°C | 1.810 ± 0.002  |
| CH <sub>3</sub> NH <sub>3</sub> PbIBr <sub>2</sub> _225°C | 1.790 ± 0.002  |

However, a common way to extract the direct gaps from optical absorption spectra is the Tauc plot, which is based on the assumption that the energy-dependent absorption coefficient  $F(R)$ , when plot a graph between  $[F(R)hv]^2$  versus photon energy ( $hv$ ) then we get a straight line. Theoretically,  $n$  equal 2 for a direct allowed transition. We examined the effect of annealing temperatures the precursor affected the optical proprieties have affect the optical band gap, while the other three dopants produced small decreases. Many research and reports tried to assign conventional or new mechanisms for the generation of carriers upon illumination. The absorption spectrum of  $MAPbI_3$  is reported (Hutter et al., 2017) with a band edge at 780 nm, band gap about 1.5 eV. This perovskite is able to absorb all of the visible spectrum. This strong optical absorption is one of the important characteristics for a photovoltaic material. Atourki (Atourki et al., 2016) reported the onset band gap of mixed bromide iodide perovskite thin films was locate in intermediate values between 1.55 eV for  $MAPbI_3$  and 2.27 eV for  $MAPbBr_3$  meaning that the band gap can be tuned by varying the composition.

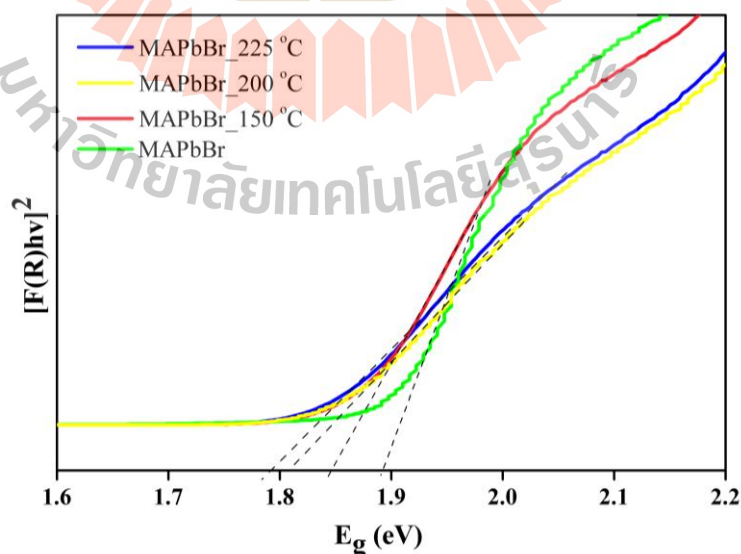


**Figure 4.7** Plot of  $[F(R)hv]^2$  versus photon energy ( $hv$ ) for the perovskites  $CH_3NH_3PbIBr_2$  compound prepared at various temperatures.

The optical band gap values are obtained by extrapolating the linear portion of the plots of  $[F(R)hv]^2$  versus  $F(R) = 0$ . As shown in Figure 4.7, the optical band gap of  $\text{CH}_3\text{NH}_3\text{PbIBr}_2$  compounds initially red shift (1.88-1.79 eV) was observed in the annealing temperature range of the as 150-225°C. The band gap calculated from the diffuse reflectance spectra using the KM function  $F(R)$  was found to be  $1.890 \pm 0.002$ ,  $1.840 \pm 0.003$ ,  $1.810 \pm 0.002$  and  $1.790 \pm 0.002$  eV with increasing annealing temperature.

#### 4.7 X-ray photoelectron spectroscopy (XPS)

Additional XPS characterization of samples is discussed in this section. Figure 4.8 show the XPS survey scan of as samples powder ( $\text{CH}_3\text{NH}_3\text{PbIBr}_2$ ) annealing between 150–400°C. The XPS information was recorded to confirm the chemical banding state in the perovskite samples. Further insight can be obtained by detailed core level analysis.

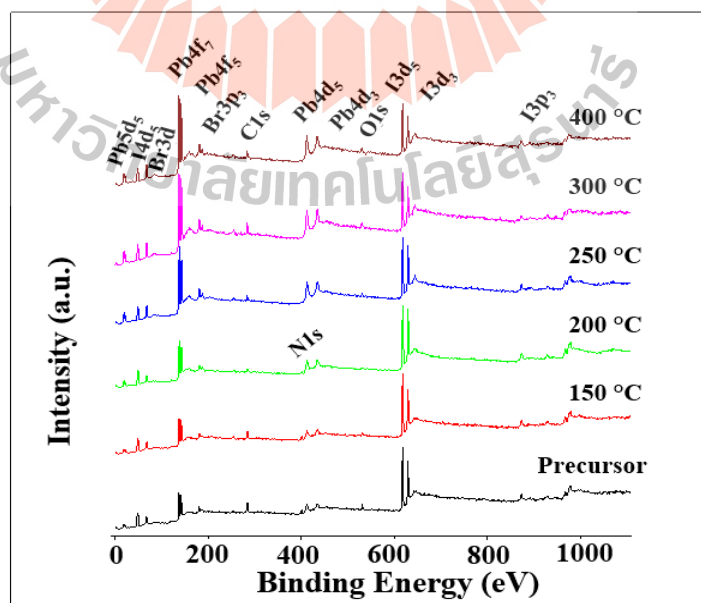


**Figure 4.8** XPS survey scan of samples.

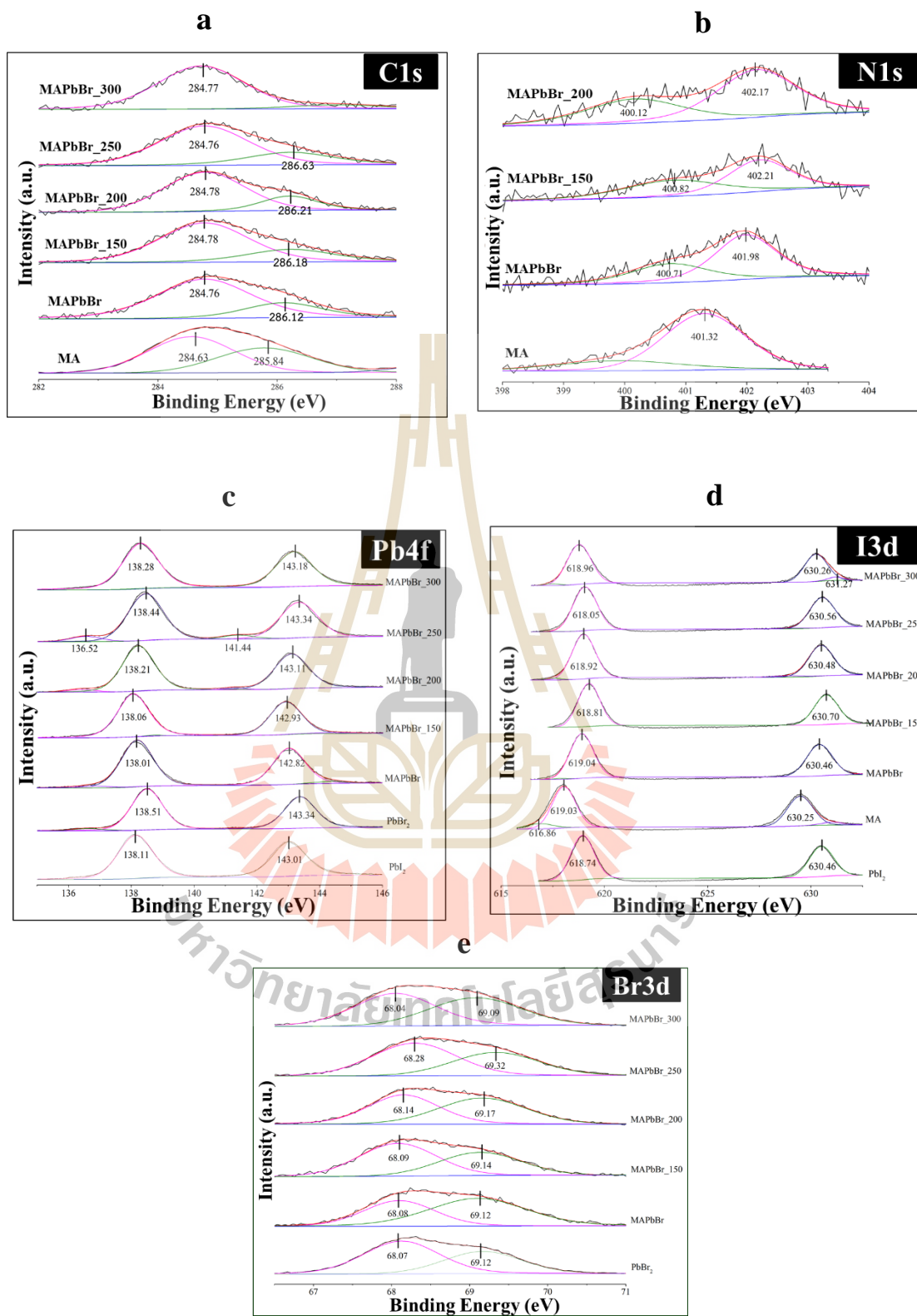
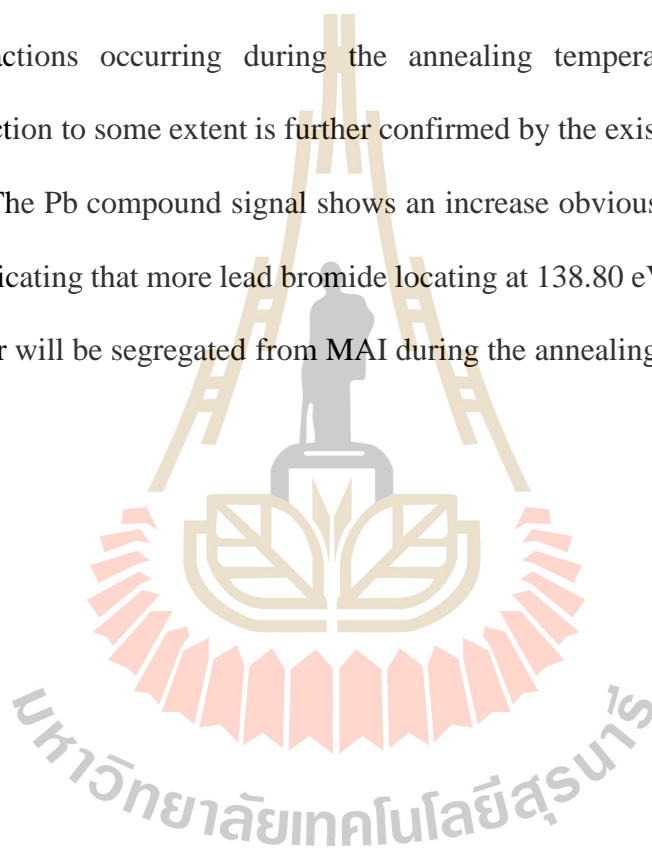


**Figure 4.9** The XPS core level peaks of samples and the Gaussian fitting for a.) C1s, b.) N1s, c.) Pb4f, d.) I3d, e.) Br3d.

In Figure 4.9a presents the XPS spectra results of material detected core level analysis. The C 1s peak consists of the carbon about 285.84 eV and a small of amorphous C contamination at 284.63 eV conventionally assigned to carbon contamination may start from the reaction with O of C-O-C contamination. For visual clarity, we normalized all the spectra to the same height. Based on the XPS result, the Figure 4.9b was revealed that the carbon peak is substantially larger than the N 1s peak from organic cation shown. The Pb 4f core level signals for different samples are shown in Figure 4.9c. The  $\text{CH}_3\text{NH}_3\text{PbIBr}_2$  sample exhibits two dominant peaks located at 138.01 eV and 142.82 eV, corresponding to the Pb 4f<sub>7/2</sub> and Pb 4f<sub>5/2</sub> level, respectively, indicating a spin-orbit splitting of 4.81 eV by the typical position and separation of spin orbit complement for  $\text{Pb}^{2+}$  and Pb metal. The small satellites at low binding energy are according to previous reports due to metallic lead. Figure 4.9d shows I signal, the spectra contain two sharp peaks at 619.04 eV and small peak at 616.86 eV corresponding to I3d<sub>3/2</sub> and I3d<sub>5/2</sub> respectively. The spectra indicate is good separated spin orbit component, the separation of around 11.42 eV being found in all the case presence of  $\Gamma$  species. Therefore, the peak of I are a shift towards higher binding energy value suggesting that small improvements are produced in the oxidation state of  $\text{I}^-$  after annealing about 0.23 eV. The Br3d peak in Figure 4.9e were fitted to two overlapping symmetric Gaussian peaks: corresponding to Br 3d<sub>3/2</sub> and Br 3d<sub>5/2</sub> peaks, are also clearly seen in the Br 3d core level, locating at 68.8 eV, following the intensity of peaks increased concomitant with the increases of temperature annealing in the sample. Moreover reported, while the optical band gap energy of annealing temperature samples increased slightly until annealing to 150°C to 200°C when the band gap decreased slightly, suggesting that the presence of the annealing temperature slightly modified the

interaction of ions in the network, leading to changes in the band gap energy value. In the case of the interactions between the dopants of  $\text{PbBr}_2$  and the MAI groups, slight modifications can be observed in the chemical bonding such as if we analyse the signals obtained for N presents the spectra of N 1s, C 1s and Br 3d core level consist a second peak as presented in the signal on annealed samples a slight shift towards a higher binding energy. Indicating that N and C part may be associated with the complex chemical reactions occurring during the annealing temperature procedure. The chemical reaction to some extent is further confirmed by the existence of the strong Pb component. The Pb compound signal shows an increase obviously after the annealing at  $200^\circ\text{C}$ , indicating that more lead bromide locating at 138.80 eV is decomposed from this sample or will be segregated from MAI during the annealing process.



# CHAPTER V

## CONCLUSIONS

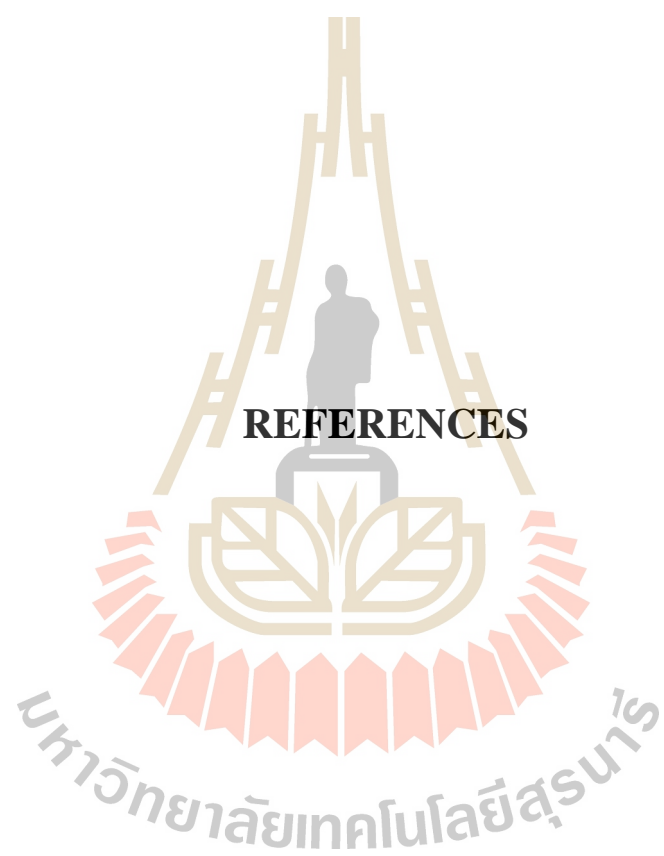
### 5.1 Conclusions

This thesis studied the effects of annealing temperature on the structure and the optical and electronic behaviors of the mixed bromide-iodide perovskites ( $\text{CH}_3\text{NH}_3\text{PbIBr}_2$ ) system. We also prepared perovskites compound by one step, solid-state reaction processes using different the annealing temperature. Reasons to using process of solid state reaction is inexpensive, low temperature and requires short processing time. We examined the mechanism of thermal degradation in the perovskite compound as a function of temperature using in TGA analysis techniques, indicates that the  $\text{CH}_3\text{NH}_3\text{PbIBr}_2$  is stable above  $< 250^\circ\text{C}$  which no found a weight loss occurred at low temperatures. The phase formation as well as crystal structure were investigated by XRD and WAXS results, we found that annealing temperature up to  $225^\circ\text{C}$  are required to achieve optimal conditions for the mixed halide perovskites structure ( $\text{CH}_3\text{NH}_3\text{PbIBr}_2$ ) and the XRF results show the atomic ratio is  $\text{Pb:I:Br} = 1:1:2$ . Furthermore, SEM images demonstrate that the samples have average particle size from 40 to  $80\ \mu\text{m}$  with increasing temperature condition of the perovskite compound from 150 to  $250^\circ\text{C}$ . Following this approach, the values of the band gap were calculated and found to decrease from 1.89 eV to 1.79 eV with increasing the annealing temperature up to  $225^\circ\text{C}$  with the report. X-ray photoelectron spectroscopy (XPS) has been used to investigate the compositional changes caused by compounds degradation.

## 5.2 Suggestions for Future Works

From the results obtained in this study, several observations from the experiments have not yet been explained. There are some questions and problems that are interesting to conduct the following studies,

1. To understand more on domain mechanisms of the mixed halide (Br with Cl) perovskites compound under thermal annealing temperature condition should be investigated.
2. To understand of the structure-property relationships of the entire hybrid material system to fabricate compounds for efficient solar cell devices.
3. One motivation of this study is to design organic molecules that have the appropriate molecular energy levels so that we could control the optical and electrical properties of the perovskite structure.
4. On the other hand, several challenges remain, of which the most critical is that PSCs suffer from poor stability.



**REFERENCES**

## REFERENCES

- Atta, N. F., Galal, A. and Ekram, H. E. (2016). Perovskite nanomaterials-synthesis, characterization and applications. **IntechOpen Access Publisher**. 6.
- Baikie, T., Fang, Y., Kadro, J. M., Schreyer, M., Wei, F., Mhaisalkar, S. G., Graetzel, M. and White, T. J. (2013). Synthesis and crystal chemistry of the hybrid perovskite  $(\text{CH}_3\text{NH}_3)\text{PbI}_3$  for solid-state sensitised solar cell applications. **Journal of Materials Chemistry**. 28.
- Ball, J. M., Lee, M. M., Hey, A. and Snaith, H. J. (2013). Low-temperature processed meso-superstructured to thin-film perovskite solar cells. **Energy & Environmental Science**. 6.
- Bernal, C. and Yang, K. (2014). First-principles hybrid functional study of the organic inorganic perovskites  $\text{CH}_3\text{NH}_3\text{SnBr}_3$  and  $\text{CH}_3\text{NH}_3\text{SnI}_3$ . **Journal of Physical Chemistry**. 24.
- Boukamp, B. A. (2003). Fuel cells: The amazing perovskite anode. **Nature Materials**. 2.
- Brivio, F., Frost, J. M., Skelton, J. M., Jackson, A. J., Weber, O. J., Weller, M. T., Goni, A. R., Leguy, A. M. A., Barnes, P. R. F. and Walsh, A. (2015). Lattice dynamics and vibrational spectra of the orthorhombic, tetragonal, and cubic phases of methylammonium lead iodide. **Physical Review**. 92.
- Burschka, J., Pellet, N., Moon, S. J., Baker, R. H., Gao, P., Nazeeruddin, M. K. and Grätzel, M. (2013). Sequential deposition as a route to high-performance

- perovskite-sensitized solar cells. **Nature**. 499.
- Chung, I., Lee, B., He, J. Q., Chang, R. P. H. and Kanatzidis, M. G. (2012). All-solid-state dye-sensitized solar cells with high efficiency. **Nature**. 486.
- Chen, L., Tang, F., Wang, Y., Gao, S., Cai, J. and Chen, L. (2015). Facile preparation of organometallic perovskite films and high-efficiency solar cells using solidstate chemistry. **Journal of Nano Research**. 8.
- Dogan, F., Lin, H., Guilloux-Viry, M. and Peña, O. (2015). Focus on properties and applications of perovskites. *Science and Technology of Advanced Materials*. 16.
- Eamesl, C., Frost1, J. M., Barnes, P. R. F., Oregan, B. C., Walshl, A. and Islam, M. S. (2015). Ionic transport in hybrid-lead iodide perovskite solar cells. **Nature Communications**. 6.
- Eperon, G. E., Stranks, S. D., Menelaou, C., Johnston, M. B., Herza, L. M. and Snaith, H. J. (2014). Formamidinium lead trihalide: a broadly tunable perovskite for efficient planar hetero junction solar cells. **Energy & Environmental Science**. 7.
- Eperon, G. E., Leijtens, T., Bush, K. A., Green, T., Wang, J. T.-W., McMeekin, D. P., Volonakis, G., Milot, R. L., Slotcavage, D. J., Beslile, R. and Snaith, H. J. (2017). Photovoltaic mixed cation lead mixed-halide perovskites links between crystallinity, photo-stability and electronic properties. **Science**. 10.
- Etgar, L., Gao, P., Xue, Z. S., Peng, Q., Chandiran, A. K., Liu, B., Nazeeruddin, M. K. and Gratzel, M. (2012). Mesoscopic  $\text{CH}_3\text{NH}_3\text{PbI}_3/\text{TiO}_2$  heterojunction solar cells. **Journal of the American Chemical Society**. 134.
- Even, L. P. J., Jancu, J. M. and Katan, C. (2013). Importance of spin-orbit coupling in hybrid organic/inorganic perovskites for photovoltaic applications. **Journal of Physical Chemistry Letters**. 4.

- Filip, M. R., Eperon, G. E., Snaith, H. J. and Giustino, F. (2014). Steric engineering of metal halide perovskites with tunable optical band gaps. **Nature Communications**. 5.
- Formhals, A. (1934). Process and apparatus for preparing artificial threads. **United States Patent**. 1.
- Formhals, A. (1944). Method and apparatus for spinning. **United States Patent**. 2.
- Fu, Y., Meng, F., Matthew, B. R., Blaise, J. T., Melinda, J. S., Dewei, M., Robert, J. H., John, C. W. and Jin, S. (2015). Solution growth of single crystal methylammonium lead halide perovskite nanostructures for optoelectronic and photovoltaic applications. **Journal of the American Chemical Society**. 17.
- Green, M. A., Ho-Baillie, A. and Snaith, H. J. (2014). The emergence of perovskite solar cells. **Nature Photonics**. 514.
- Greiner, A. and Joachim, H. W. (2007). Electrospinning: a fascinating method for the preparation of ultrathin fibers. **Angewandte Chemie**. 46.
- Hao, Q., Chua, Y., Zhengb, X., Liua, Z., Lianga, L., Qic, J., Zhanga, X., Liud, G., Liua, H., Chena, H. and Liu, C. (2016). Preparation of planar  $\text{CH}_3\text{NH}_3\text{PbI}_3$  thin films with controlled size using 1-ethyl-2-pyrrolidone as solvent. **Journal of Alloys and Compounds**. 11.
- Heo, J. H., Song, D. H. and Im, S. H. (2014). Planar  $\text{CH}_3\text{NH}_3\text{PbBr}_3$  hybrid solar cells with 10.4% power conversion efficiency, fabricated by controlled crystallization in the spin-coating process. **Advanced Materials**. 26.
- Horváth, E., Spina, M., Szekrényes, Z., Kamarás, Gaal, K., Gachet, R. D. and Forró, L. (2014). Nanowires of methylammonium lead iodide ( $\text{CH}_3\text{NH}_3\text{PbI}_3$ ) prepared by low temperature solution-mediated crystallization. **Nano Letters**. 12.

- Huang, J., Jiang, K., Cui, X., Zhang, Q., Gao, M., Su, M., Yang, L. and Song, Y. (2015). Direct conversion of  $\text{CH}_3\text{NH}_3\text{PbI}_3$  from electrodeposited  $\text{PbO}$  for highly efficient planar perovskite solar cells. **Scientific Reports**. 5.
- Im, J. H., Kim, H. S. and Park, N. G. (2014). Morphology-photovoltaic property correlation in perovskite solar cells: one-step versus two-step deposition of  $\text{CH}_3\text{NH}_3\text{PbI}_3$ . **Applied Physics Letters Materials**. 2.
- Im, J. H., Lee, C. R., Lee, J. W., Park, S. W. and Park, N. G. (2011). 6.5% Efficient perovskite quantum-dot-sensitized solar cell. **Nanoscale**. 3.
- Im, J. H., Luo, J., Franckevičius, M., Pellet, N., Gao, P., Moehl, T., Zakeeruddin, S. M., Nazeeruddin, M. K., Grätzel, M. and Park, N. G. (2015). Nanowire perovskite solar cell. **Nano Letters**. 15.
- Jacobsson, T. J., Pazoki, M., Hagfeldt, A. and Edvinsson, T. (2015). Goldschmidt's rules and strontium replacement in lead halogen perovskite solar cells: theory and preliminary experiments on  $\text{CH}_3\text{NH}_3\text{SrI}_3$ . **Journal of Physical Chemistry**. 119.
- Jeon, N. J., Noh, J. H., Yang, W. S., Kim, Y. C., Ryu, S., Seo, J. and Seok, S. I. (2015). Compositional engineering of perovskite materials for high-performance solar cells. **Nature**. 476.
- Jung, H. S. and Park, N. G. (2015). Perovskite solar cells: from materials to devices. **Materials Views**. 11.
- Kagan, C. R., Mitzi, D. B. and Dimitrakopoulos, C. D. (1999). Organic-inorganic hybrid materials as semiconducting channels in thin-film field-effect transistors. **Science**. 286.
- Kieslich, G., Sun S., Im, J. H. and Cheetham, A. K. (2015). An extended tolerance factor approach for organic-inorganic perovskites. **Chemical Science**. 6.

- Kim, H. S., Lee, C. R., Im, J. H., Lee, K. B., Moehl, T., Marchioro, A., Moon, S. J., Baker, R.H., Yum, J. H., Moser, J. E., Grätzel, M. and Park, N. G. (2012). Lead iodide perovskite sensitized all solid-state submicron thin film mesoscopic solar cell with efficiency exceeding 9%. **Scientific Reports**. 2.
- Kitazawa, N., Watanabe, Y. and Nakamura, Y. (2002). Optical properties of  $\text{CH}_3\text{NH}_3\text{PbX}_3$  (X= halogen) and their mixed-halide crystals. **Journal of Materials Science**. 37.
- Knop, O., Wasylishen, R. E. and Oort, M. J. M.V.(1990). Alkylammonium lead halide. Part 2.  $\text{CH}_3\text{NH}_3\text{PbX}_3$  (X= Cl, Br, I) perovskite cuboctahedral halide cage with isotropic cation reorientation. **Canadian Journal of Chemistry**. 68.
- Knutson, J. L., Martin, J. D. and Mitzi, D. B. (2005). Tuning the band gap in hybrid tin iodide perovskite semiconductors using structural templating inorg. **Chemistry**. 44.
- Kojima, A., Teshima, K., Shirai, Y. and Miyasaka, T. (2009). Organometal halid perovskites as visible-light sensitizers for photovoltaic cells. **Journal of the American Chemical Society**. 17.
- Kojima, A., Ikegami, M., Teshima, K. and Miyasaka, T. (2012). Highly luminescent lead bromide perovskite nanoparticles synthesized with porous alumina media. **Chemistry Letters**. 41.
- Kollek, T., Gruber, D., Gehring, J., Zimmermann, E., Mende, L. S. and Polarz, S. (2015). Porous and shape-anisotropic single crystals of the semiconductor perovskite  $\text{CH}_3\text{NH}_3\text{PbI}_3$  from a single-source precursor. **Angewandte Chemie**. 54.

- Kresse, G. and Furthmuller, M. (1996). Efficient iterative schemes for ab initio total-energy calculations using a plane-wave basis set. **Physical Review Journals**. 54.
- Kumar, V. B., Gouda, L., Porat, Z. and Gedanken, A. (2014). Sonochemical synthesis of  $\text{CH}_3\text{NH}_3\text{PbI}_3$  perovskite ultrafine nanocrystal sensitizers for solar energy applications. **Ultrasonics Sonochemistry**. 32.
- Lee, M. M., Teuscher, J., Miyasaka, T., Murakami, T. N. and Snaith, H. J. (2012). Efficient hybrid solar cells based on meso-superstructured organometal halide perovskites. **Science**. 338.
- Lee, M. M. and Jun, Y. (2015). Efficient fiber-shaped perovskite photovoltaics using silver nanowires as top electrode. **Journal of Materials Chemistry**. 3.
- Li, Z. H., Liu, J., Ma, J. Y., Jiang, Y., Ge, Q. Q., Ding, J., Hu, J. S. and Wan, L. J. (2016). Solvent-assisted preparation of high performance mesoporous  $\text{CH}_3\text{NH}_3\text{PbI}_3$  perovskite solar cells. **Journal of Nanoscience and Nano - technology**. 16.
- Liu, M., Johnston, M. B. and Snaith, H. J. (2013). Efficient planar hetero junction perovskite solar cells by vapour deposition. **Nature**. 501.
- Mitzi, D. B. (1996). Synthesis, crystal structure, and optical and thermal properties of  $(\text{C}_4\text{H}_9\text{NH}_3)_2\text{MI}_4$  (M= Ge, Sn, Pb). **Chemistry of Materials**. 8.
- Mitzi, D. B., Feild, C. A., Schlesinger, Z. and Laibowitz, R. B. (1995). Transport, optical, and magnetic properties of the conducting halide perovskite  $\text{CH}_3\text{NH}_3\text{SnI}_3$ . **Journal of Solid State Chemistry**. 114.
- Mitzi, D. B., Wang, S., Feild, C. A., Chess, C. A. and Guloy, A. M. (1995). Conducting layered organic-inorganic halides containing  $\langle 110 \rangle$  oriented perovskite sheets. **Science**. 267.

- Mitzi, D. B. (2000). Organic-inorganic perovskites containing trivalent metal halide layers: the templating influence of the organic cation layer inorg. **Chemistry**. 39.
- Moller, C. K. (1958). Crystal structure and photoconductivity of cesium plumb halides. **Nature**. 182.
- Mosconi, E., Amat, A., Nazeeruddin, M. K., Gratzel, M. and De Angelis, F. (2013). First-principles modeling of mixed halide organometal perovskites for photovoltaic applications. **Journal of Physical Chemistry C**. 117.
- Nguyen, M. T., Vu, T. V. P., Bui, B. T., Luong, T. T., Nguyen, M. H., Ngoc, L. H., Bui, V. D., Truong, T. T. and Thuat, N. T. (2015). Optical and structural study of organometal halide materials for applications in perovskite-based solar cells. **Journal of Electronic Materials**. 45.
- Noel, N. K., Stranks, S. D., Abate, A., Wehrenfennig, C., Guarnera, S., Haghighirad, A.-A., Sadhanala, A., Eperon, G. E., Pathak, S. K., Johnston, M. B., Petrozza, A., Herz, L. M. and Snaith, H. J. (2014). Lead-free organic-inorganic tin halide perovskites for photovoltaic applications. **Energy & Environmental Science**. 3061.
- Noh, J. H., Im, S. H., Heo, J. H., Mandal, T. N. and Seok, S. I. (2013). Chemical management for colorful, efficient, and stable inorganic-organic hybrid nanostructured solar cells. **Nano Letters**. 4.
- Norton, C. L. (1936). Method and apparatus for fibrous or filamentary material. **United States Patent**. 61.
- Park, N. G. (2013). Organometal perovskite light absorbers toward a 20% efficiency low-cost solid-state mesoscopic solar cell. **Journal of Physical Chemistry Letters**. 4.

- Piskunov, S., Heifets, E., Eglitis, R. I. and Borstel, G. (2004). Bulk properties and electronic structure of SrTiO<sub>3</sub>, BaTiO<sub>3</sub>, PbTiO<sub>3</sub> perovskites: an ab initio HF/DFT study. **Computational Materials Science**. 29.
- Pena, M. A. and Fierro, J. L. G. (2001). Chemical structures and performance of perovskite oxides. **Chemical Reviews**. 101.
- Saliba, M., Matsui, T. S., Domanski, J. Y. K., Correa, B. J. P., Nazeeruddin, M. K., Zakeeruddin, S.M., Tress, W., Abate, A., Hagfeldt, A. and Grätzel, M. (2016). Cesium-containing triple cation perovskite solar cells: improved stability, reproducibility and high efficiency. **Energy & Environmental Science**. 12.
- Schmidt, L. C., Pertegas, A., Carrero, S. G., Malinkiewicz, O., Agouram, S., Espallargas, G. M., Bolink, H. J., Galian, R. E. and Prieto, J. P. (2014). Non-template synthesis of CH<sub>3</sub>NH<sub>3</sub>PbBr<sub>3</sub> perovskite nanoparticles. **Journal of the American Chemical Society**. 3.
- Schokley, W. and Queisser, H. J. (1961). Detailed balance limit of efficiency of p-n junction solar cells. **Journal of Applied Physics**. 32.
- Snaith, H. J. (2013). Perovskites: the emergence of a new era for low-cost, high-efficiency solar cells. **Journal of Physical Chemistry Letters**. 3623.
- Spina, M., Bonvin, E., Sienkiewicz, A., Náfrádi, B., Forró, L. and Horváth, E. (2016). Controlled growth of CH<sub>3</sub>NH<sub>3</sub>PbI<sub>3</sub> nanowires in arrays of open nano fluidic channels. **Scientific Reports**. 6.
- Stranks, S. D., Eperon, G. E., Grancini, G., Menelaou, C., Alcocer, M. J. P., Leijtens, T., Herz, L. M., Petrozza, A. and Snaith, H. J. (2013). Electron-hole diffusion lengths exceeding 1 micrometer in an organometal trihalide perovskite absorber. **Science**. 342.

- Tai, Q., You, P., Sang, H., Liu, Z., Hu, C., Chan, H. L. W. and Yan, F. (2016). Efficient and stable perovskite solar cells prepared in ambient air irrespective of the humidity. **Nature Communications**. 7.
- Wan, J. Y., Tingting, S. and Yanfa, Y. (2014). Unusual defect physics in  $\text{CH}_3\text{NH}_3\text{PbI}_3$  perovskite solar cell absorber. **Journal of Physical Chemistry Letters**. 104.
- Wang, Z., Zhang, B., Otsuka, T., Inoue, K., Kobayashi, H. and Kurmood, M. (2004). Anionic NaCl-type frameworks of  $[\text{MnII}(\text{HCOO})^3^-]$ , templated by alkyl ammonium, exhibit weak ferromagnetism. **Dalton Transactions**. 15.
- Wang, F., Grinberg, I. and Rappe, A. M. (2014). Band gap engineering strategy via polarization rotation in perovskite ferroelectrics. **Applied Physics Letters**. 104.
- Weber, D. (1978).  $\text{CH}_3\text{NH}_3\text{PbX}_3$ , a Pb(II)-system with cubic perovskite structure. **Zeitschrift für Naturforschung B**. 33.
- Weber, D. (1978).  $\text{CH}_3\text{NH}_3\text{SnBr}_x\text{I}_{3-x}$  ( $x= 0- 3$ ), a Sn(II)-system with cubic perovskite structure. **Zeitschrift für Naturforschung B**. 34.
- Weber, D. (1979). The perovskite system  $\text{CH}_3\text{NH}_3[\text{Pb}_n\text{Sn}_{1-n}\text{X}_3]$  ( $X= \text{Cl}, \text{Br}, \text{I}$ ). **Zeitschrift für Naturforschung B**. 35.
- Xia, H. R., Sun, W. T. and Peng L. M. (2015). Hydrothermal synthesis of organometal halide perovskites for Li-ion batteries. **Chemical Communications**. 51.
- Xing, G.C., Mathews, N., Sun, S. Y., Lim, S. S., Lam, Y. M., Gratzel, M., Mhaisalkar, S. and Sum, T. C. (2013). Long-range balanced electron and hole-transport lengths in organic-inorganic  $\text{CH}_3\text{NH}_3\text{PbI}_3$ . **Science**. 342.
- Yamamuro, N. O., Matsuo, O. and Suga, H. (1996). Heat capacities and phase transitions of protonated and deuterated methylammonium tetra fluoroborates. **The Journal of Physical Chemistry**. 100.

## CURRICULUM VITAE

Name: Miss. Wipakorn Rittisut

Date of birth: 6 December 1992

Place of birth: Ubon Ratchathani, Thailand

Nationality: Thai

### Education

Academic year

2011-2014 Ubon Ratchathani University, Ubon Ratchathani, Thailand.

Bachelor of Science (Physics)

2014-2018 Suranaree University of Technology, Nakhon Ratchasima,  
Thailand.

Master of Science (Physics)

มหาวิทยาลัยเทคโนโลยีสุรนารี

